Normalised behaviour of a non-plastic silt-pumice sand mixture

L. Zuo[a,#], B.A. Baudet[b]

[a]Department of Civil Engineering, School of Human Settlements and Civil Engineering, Xi'an Jiaotong University, Xi'an, China; formerly The University of Hong Kong

[b]Department of Civil, Environmental and Geomatic Engineering, University College London

[#]corresponding author

Abstract

The existence and failures of silty sand have been reported worldwide, and the behaviour of sand-silt mixtures at small to large strains has been intensively studied. Due to the relatively low stress level achieved in laboratory testing, no unifying framework has yet been proposed for sand-silt mixtures. In the presented work, a crushable sand, made of pumice, was used as host sand so as to reach a unique Normal Compression Line under pressures easily attainable in the laboratory. The sand was combined with non-plastic fines in proportions varying between 0% and 100%, and tested in compression and shearing with associated bender element testing for small strain stiffness measurements. The unique relationship between pressure and volume on the Normal Compression Line allowed for the normalisation of the data in a way that highlights the effects of fines irrespective of the density. It was found that once the effects of the fines on the index properties and compressibility have been cancelled, by normalising for volume, the behaviour of the sand-silt mixtures can be characterised as unique.

Keywords

Dynamics, Laboratory tests, Sands, Silts, Stiffness, Strain

Introduction

The behaviour of non-plastic fines-sand mixtures has been extensively researched, experimentally (e.g. Lade et al., 1998; Salgado et al., 2000; Polito & Martin, 2001; Georgiannou, 2006; Yang et al., 2006; Dash et al., 2010; Carrera et al., 2011; Wichtmann et al., 2015; Goudarzy et al., 2016a,b; Zuo & Baudet, 2015; Yang & Liu, 2016; Liu & Yang, 2018), and numerically (e.g. Voivret et al., 2009; Minh et al., 2014; To et al., 2014; Shire et al., 2014; 2016). Previous experimental studies were for the majority carried out at low pressures where the compression curve depends on the initial density. This means that they remain, despite their number, isolated, and that no unifying framework has yet been proposed in the same way as for sands. It has been shown that Critical State Soil Mechanics can be applied to sands (e.g. Coop, 1990), and it was made possible by carrying out tests on sands to high pressures so that they reached a unique Normal Compression Line (NCL), where a unique relationship between pressure and volume can be found in the v-lnp' plane. It can also be expressed in the ln$v$-lnp' plane (Butterfield, 1979), where it is usually given by

$$\ln v = \mathrm{N}^* - \lambda^* \ln p' \quad [1]$$

where v is the specific volume, p' is the mean effective stress, λ^* is the gradient and N^* is the intercept of the NCL at p'=1kPa. Particularly, this is important for normalization, for example, the normalization of volume to determine effects of overconsolidation ratio on the small strain stiffness (e.g. Jovičić & Coop, 1997). At low pressures, the void ratio (or density) must be considered separately from the stress level to define the soil state; an illustration is the empirical equation proposed by Ishihara (1996) which links small strain stiffness in sand to stress and void ratio. On the other hand, when on a unique Normal Compression Line, only one of the two variables, stress or void ratio, is enough to define the soil state and the equation is simplified so that the stiffness is a simple power function of stress (e.g. Jovičić & Coop, 1997).

Of the recently published papers on the effect of fines on sand behaviour, most mixtures investigated had a gradation gap wide enough so that the concepts of inter-granular and inter-fines could be applied (i.e. a ratio of coarse to fine diameters equal or larger than 6.5; Thevanayagam et al., 2002). An equivalent criterion was proposed by Kenney and Lau (1985) for filters, where the particle size ratio larger than 4 leads to instability. A large amount of work has been carried out at very small strains to investigate the effect of non-plastic fines on the dynamic shear modulus. New expressions for the small strain stiffness of silty sand have been proposed: Wichtmann et al. (2015) and Goudarzy et al. (2018a) suggests a function of stress and global void ratio with fitting parameters or reduction factor related to fines content; Goudarzy et al. (2016a) suggested a function of stress and the equivalent intergranular void ratio defined by Thevanayagam et al. (2002), while Yang & Liu (2016) suggested a function of stress and the state parameter defined by Been & Jefferies (1985). The need to consider a function of either global void ratio, state parameter, or intergranular void ratio in addition to pressure stems from the fact that these studies were carried out at stress levels too low to reach a unique relationship between pressure and volume. By carrying out tests at pressures high enough to reach a unique NCL, the uncertainty about the void ratio function becomes redundant. Recent studies on the behaviour of silty sands at larger strains have been done mostly within the context of transitional soils for which the initial density has a strong influence on the mechanical response, for example the location of the Normal Compression Line and Critical State Line depend on the initial void ratio (Shipton & Coop, 2015). It was however found that if the larger particles are weaker than the fines, the soil behaves as predicted by Critical State Soil Mechanics, with unique Normal Compression and Critical State Lines (Ponzoni et al., 2017).

Reaching the unique NCL in sands is usually accompanied by particle breakage (e.g. Lee & Coop, 1995; Vilhar et al., 2013). The method adopted in the work presented here was to use a crushable sand as host sand in non-plastic fines-sand mixtures, which can reach a unique Normal Compression Line under pressures easily attainable in the laboratory. It was thus possible to normalise the data in a way that highlights the effects of fines irrespective of the density. This is a valuable advantage since adding fines has the clear effect of affecting the absolute and relative density (e.g. Zuo & Baudet, 2015).

Materials, testing apparatus and procedures

Materials

Pumice is a typical lightweight porous volcanic rock formed during explosive volcanic eruptions, which is considered to be more crushable than other sands due to its vesicular nature (e.g. Liu et al., 2016). In this research, manufactured pumice sand shipped from New Zealand was first sieved; the particles remaining between the sieves of 0.6mm and 1.18mm were then collected as the host sand for further experiments. A measured specific gravity of 2.09 suggests the existence of pores inside the particle. A relatively irregular shape and rough surface can be observed in SEM images (figure 1a), while results from Qicpic dynamic image analysis indicate a mean particle size D_{50} of 0.942mm and shape factors with rather low values: mean aspect ratio, 0.72; mean convexity, 0.94; and mean sphericity, 0.83. Crushed silica silt was chosen as the fine fractions. It has a wide range of particle sizes, from 2 to 60μm, with a mean particle size d_{50} of 14μm. The ratio of sand to silt diameter is therefore 67, well in excess of the recommended value of 6.5 for intergranular void ratios to apply (Thevanayagam et al., 2002). The SEM images of silt particles (figure 1b) show an angular shape. The specific gravity is 2.60.

Index properties

Void ratio indices of sand-fines mixtures are usually changing with fines content. The index properties e_{max} and e_{min} of mixtures are important since they indicate a possible range where a transitional fines content, FC_t, may exist (Zuo & Baudet, 2015), which forms a reference value for further experimental work. A simplified method suggested by Muszynski (2006) was used to determine e_{max} and e_{min} of the pumice-silt mixtures with different fines contents, each fines content calculated as the weight of silt over the total weight of the mixture. An alternate mold with inner diameter of 40mm and height of 75mm was used after volume calibration with water, and a funnel was used when placing the mixtures into the mold with great caution to avoid segregation. In addition, in the e_{min} test, a surcharge of 11.8kpa was applied and a dowel was used to tap the midpoint of the mold for the densification process. The results, shown in figure 2, highlight a clear transitional behaviour, with FC_t around 50-60%. The value of e_{max} reaches its lowest point earlier than e_{min}, although e_{min} decreases at a faster rate until the FC_t is reached, then increases slower than e_{max} afterwards. This may be because in the e_{max} condition, not all the fine particles are filling the voids between large particles even when the fines content is small, so that there are always fines separating sand particles apart, while the applied dead weight and vibration used when determining e_{min} may cause more fine particles to fill in the voids, which leads to a larger FC_t. Usually, different experimental methods will give a possible range where FC_t exists (Zuo & Baudet, 2015; Goudarzy et al., 2016b), while here between e_{max} and e_{min}, the value of FC_t determined from e_{min} is preferred since the e_{min} condition is closer to the theoretical interpretation proposed by Lade et al. (1998), that is FC_t can be reached when all fine particles fill the voids between sand particles without breaking the sand-sand contacts.

Based on the FC_t obtained from void ratio indices, which is estimated to be around 50%, pumice-silt mixtures with 0, 30, 50, 60, and 100% fines content were tested. One-dimensional compression, isotropic compression, and triaxial shearing tests were conducted to study the medium to large strain behaviour of the mixtures, in combination with bender element tests to characterise the small-strain behaviour under different stress and state conditions.

Testing apparatus and procedures

Before tests, the oedometer and triaxial cells, loading frames, and pressure controllers were all validated, and the transducers, including load cell, water pressure transduce, and LVDTs were all calibrated. Moist tamping method was used for specimen preparation. The sand and silt particles were first weighed according to the designed silt content and initial void ratio, and then well-mixed at an initial water content of 5% to achieve mixtures with homogeneous fabric. Then the mixtures were compacted in layers to prepare the specimens in proper sizes for compression and shear testing. After tests, the sand particles were collected, oven dried, sieved and the particle size distribution was determined to analyse particle breakage.

The one-dimensional compression tests were conducted in a conventional oedometer cell with a sample size of 50mm in diameter by 20mm in height. The specimens were submerged and left overnight for saturation before the loading stages started. The deadweight was added in steps, and a maximum vertical stress of around 6.5MPa was applied. The initial sample height was determined both before and after loading independently, and used to calculate the initial void ratio. An average was taken, and calculated void ratios outside a ±0.02 range from the mean value were discarded. This was done to ensure the accuracy of the location of the NCLs on the e-lnσ'_v or e-lnp' plane (e.g. Rocchi & Coop, 2014).

The isotropic compression tests were conducted in a GDS triaxial apparatus equipped with a pair of vertical bender elements, and on specimens of 50mm diameter by 100mm height. The specimens were first flushed with CO_2 and de-aired water, and then saturated with back pressure to achieve a B-value above 0.95. After saturation, the specimens were consolidated to different effective stress levels in stages, and the maximum effective isotropic stress applied was 1.6MPa.

The GDS triaxial apparatus with a pair of vertical bender elements was also used for some shearing tests. In parallel, a conventional triaxial apparatus with sample sizes of 38mm in diameter by 76mm in height was used to identify additional stress paths and critical state points. The specimens were saturated with the same procedures as for the isotropic compression specimens. After fully consolidated under the designed isotropic effective stress, most specimens were sheared strain controlled under drained or undrained conditons, while some specimens were sheared stress controlled under constant p' condition. The shear strain rate was 0.5%/min for undrained test, and 0.05%/min for drained test. The specimens were mostly sheared to 25% strain where the deviatoric stress, pore water pressure or back volume were mostly found to be constant and which was considered as the critical state. The thickness of membrane used was 0.25mm, and the barrelling area correction and membrane correction were done when analysing shearing data.

The bender element tests were conducted during isotropic compression tests when the specimen volume became stable at each stress level, and also during the shearing tests. After necessary validation, "Agilent 33210A 10MHz Waveform Generator" was used as signal generator with a maximum applied voltage of 10V. "Agilent InfiniiVision DSO6014A Oscilloscope" was used to receive signals, both high and low frequency rejection was used to reduce the noise, and an average of 256 received signals was used to reduce the noise and increase the signal resolution. Two local LVDTs with amplifiers were installed on the sample to determine the travel distance: the measure range was 0−15mm and the resolution was ±0.0001mm. The two main methods generally used for the determination of travel time were considered: time-domain and frequency-domain method. Camacho-Tauta et al. (2015) reported that results using the time-domain method are in good agreement with the resonant column measurements, while results from frequency-domain are not. By DEM simulation, O'Donovan et al. (2015) reported that the frequency-domain method could lead to unreasonable results. It was also found in this study that the frequency-domain method did not give a satisfying performance, thus the small-strain stiffness results shown here were all determined using the time-domain method, more specifically the first arrival method. The time delay between transmitter and receiver elements was calibrated by "tip to tip" method, and to minimize the uncertainty brought by near-field effect, a series of sinusoidal input signals of frequencies from 5-15kHz were used, and a common travel time was obtained by comparing all the received signals. More detailed information of tests conducted is summarized in Table 1.

Compression behaviour

The compression curves obtained from the isotropic tests and from the oedometer tests, which reached higher pressures, are shown for the clean pumice sand and pumice-silt mixtures with 30% and 50% silt (figure 3), together with the fitted normal compression lines determined from the data points after yielding. The data are plotted in a double logarithmic graph, and the specific volume v is used instead of global void ratio e, following Butterfield's (1979) suggestion but also for the purpose of normalizing later on. It shows that for clean pumice sand, the curves yield around a mean effective stress of 600kPa. For mixtures with 0% and 30% silt, although slightly scattered data can be observed at the end of oedometer tests, compared to the volume difference at the beginning of the tests, there is clear convergence trend towards a single normal compression line (NCL). While for the mixtures with 50% silt, the data are less clear, but the samples should be compressed to higher pressures to confirm whether there is convergence, or whether the curves remain parallel as can be found in some silty sands, albeit for much smaller fines contents generally (e.g. Shipton & Coop, 2012). The steep part of the NCL is usually associated with the location where particle breakage may become significant in sand (e.g. Lee & Coop, 1995; McDowell & Bolton, 1998). Whereas most sands, in particular of quarzitic nature, only yield at very large pressures, the compression results show that the use of a crushable sand as host soil enables characterising the steep part of the NCL at regular engineering pressures. A summary of the lines determined is plotted in figure 4. The lines move downwards (decreasing values of ln$v$) with silt content, and seem to reach a lower bound at contents around 50-60%, after which they move upwards (increasing values of ln$v$). This coincides with the troughs observed in the index void ratios in figure 2, suggesting a transitional fines content around 50-60%. It indicates that the FC_t value can be determined with the variation of NCLs location, which is in agreement with the former researches (e.g. Carrera et al., 2011; Vilhar et al., 2013).

Shearing behaviour

The specimens were sheared drained or undrained at different confining stresses, from states before reaching or on the normally compression line. The tests were stopped when a stable state was reached. An example is shown in figure 5 for specimens prepared with 0%, 50% and 60% silt content under similar relative densities D_r, and the initial mean effective stress p' for all four tests were 200kPa. Constant volume (fig.5a) or pore water pressure (fig. 5b) were reached at large strains as well as a constant stress ratio (fig. 5c), enabling the determination of critical state points. Figure 5a shows that under similar initial D_r and p' in drained shearing, adding silts makes the mixtures less contractive, this is mainly due to the high crushing potential of pumice sand, which leads to a highly contractive behaviour in drained shearing, while more silts will help prevent the sand particles from breaking. Figure 5b shows that under similar initial D_r and p' in undrained shearing, adding silts makes the mixtures more contractive, which is consistent with former studies (e.g. Lade & Yamamuro, 1997). Figure 5c shows that for a given fines content, a unique stress ratio is obtained at critical state. The critical state points obtained from all the tests are plotted in the stress plane q-p' in figure 6a and in the volumetric plane ln$v$-lnp' in figure 6b. For the latter, an exponential law curve following Gudehus (1996) was chosen to fit the shallow curved part at lower stresses, while a steep, straight line was fitted to the higher stress points. The data were such that it was possible to choose the steep part of the CSL to be parallel to the NCL, as per the Critical State Framework. The effect of the silt content on its gradient, M, from the q-p' plot, and the slope and intercept of its steep part, λ^* and Γ^* respectively, from the ln$v$-lnp' plot, is highlighted in figure 7. The variation of N^*, the intercept of the NCL from the ln$v$-lnp' plot, with silt content is also shown in figure 7. It shows that the value of M increases slightly from 1.57 to 1.63 as the silt content increases to 50%, and then decreases clearly to 1.25 at 100% silt content. It indicates that the silt starts to have significant influence on the critical state friction angle when the mixture turns to "fines-dominated", and the sand particles make a major contribution before that. The values of λ^*, Γ^* and N^* all decrease immediately as the silt content starts increasing until FC_t is reached, and then increase slightly afterwards. It indicates that the silt has a significant influence on the compressibility of the mixtures, and also the volumetric response at critical state, especially when the mixture is "sand-dominated". These parameter values are used following Klotz & Coop's (2002) approach to normalise the shearing stress paths for volume and composition in figure 8. The mean effective stress p' is normalised with $p'_{cs}{}^*$, which is the projected p' on the CSL at the given ln$v$; and the deviatoric stress q is normalised with the product of $p'_{cs}{}^{*}$ and gradient M. It shows that the intercepts and gradients found from figure 7 are appropriate to normalise the stress paths, which start from isotropic states and end up at critical state, represented by a single point. Ideally the curves should be coincident, and the small scatter observed in the data will be reflected later when attempting further normalisation.

Particle breakage

Manual sieving after the compression and shearing tests allowed identifying changes in particle size distribution (e.g. for 50% fines content in fig. 9), and hence the occurrence of particle breakage. The data plotted, for sizes above 63μm, highlight the breakage endured by the pumice sand grains. It is clear that even at large fines content, the particles of pumice sand did crush significantly. The stable states found in figure 5 may thus be resulting from the cancelling out of the two mechanisms for particle re-arrangement and particle breakage at large strains (Chandler, 1985). Similarly to other sands, uniformly or well graded, the particle breakage does not affect the angle of friction at critical state (e.g. Coop et al., 2004; Altuhafi & Coop, 2011). The stable volume and pore water pressure at the end of shearing also imply that the location of the CSL in ln$v$-lnp' is not affected.

Small strain behaviour

Bender element tests were carried out during both isotropic compression and shearing. The effects of adding fines on the small strain stiffness G_0 on the normal compression and critical state lines are discussed below. In order to discard any possible effect of anisotropy induced during shearing on the small strain shear moduli, bender element tests were also carried out during constant p' tests during which the small strain stiffness was measured for vertical and horizontal directions of propagation and polarisation.

Effect of fines on G_0 on NCL and CSL

Previous studies on the effect of fines on the small strain stiffness during isotropic compression have generally been made with low fines contents (less than 30%) and at low stresses (i.e. on the curved part of the NCL). Results from bender element tests suggest a decrease in small strain stiffness with increasing fines content for a given relative density and stress level; for example data from tests on Ottawa sand-silica fines mixtures, with fines content and isotropic confining pressure up to 20% and 500kPa respectively (Salgado et al., 2000), or data from tests on mixtures of Toyoura sand and crushed silica, with fines content and isotropic confining stress up to 30% and 500kPa respectively (Yang & Liu, 2016). Similar trends were found in tests using the resonant column, typically on silica sand and fines mixtures, with fines contents up to 40% while the maximum isotropic stress was less than 850kPa (Goudarzy et al., 2016b; Payan et al., 2017). Studies on the effect of fines on the small strain stiffness during shearing are limited in comparison. Prashant et al. (2019) measured small strain stiffness of Ganga sand with different silt fines contents (2, 10, 30, 70, 100%) during undrained shearing after consolidation to 300kPa isotropic confining stress. They reported that the small strain stiffness at a given shear strain decreases with the increase of fines content, but the small strain stiffness at different stresses on the critical state line was not investigated.

Figure 10 shows bender element data of small strain stiffness obtained during isotropic compression and at critical state for the pure sand and silt-sand mixtures. The data points tend towards a unique line marking isotropic compression states for stresses in excess of about 500kPa, indicating the normal compression line in $\ln G_0$-$\ln p'$ plane. Similarly, a unique line identifying critical states can be found at those higher stress levels, which plots lower than the isotropic normal compression line, indicating the critical state line in $\ln G_0$-$\ln p'$ plane. The CSL in $\ln G_0$-$\ln p'$ was chosen to plot parallel to the NCL; although the R^2 value is relatively low due to lack of data points at higher stresses, it fits the data rather well. The distance between the two lines is more marked than what was reported on clay, for example by Viggiani & Atkinson (1995) when they investigated effects of stress-induced anisotropy on the G_0 of kaolin. We can describe the two lines (NCL and CSL) in a $\ln G_0$-$\ln p'$plane with equations of the form:

$$\frac{G_0}{p_r} = A\left(\frac{p'}{p_r}\right)^n \qquad [2]$$

as suggested by Jovičić & Coop (1997) for sands, where n and A are soil parameters, and p_r is a reference stress. The two lines (NCL and CSL) have the same slope, n, but different intercepts. Values of n = 0.8, and A_{NCL} = 703 and A_{CSL}/A_{NCL} =0.72 were found for p_r = 1kPa.

In order to differentiate possible effects of stress-induced anisotropy from effects of adding fines, constant p' shear tests were performed on pumice-silt mixtures with 0, 30, 50 and 60% fines content, combined with small strain stiffness G_0 measurement. The mean effective stress p' was kept 400kPa for all tests. Valued of G_0 at different stress ratio η (q/p') are shown in figure 11. For all mixtures, G_0 remained constant until the ratio η exceeded the value about 1.2, which generally corresponds to an axial strain less than 3% (Fig 5c). It then turned to decrease clearly afterwards as the ratio η increased further and the axial strain reached about 10%. Similar behaviour was found in the conventional drained and undrained shear tests of the pumice-silt mixtures: as the specimen was sheared to a relatively high strain level to reach the critical state, the small strain stiffness started to decrease although the mean effective stress p' was still increasing. The decrease in G_0 coincides with an acceleration in the development of shear strains, especially near the critical state. Prashant et al. (2019) found similar behaviour in their study on silty sand, but it has not been clearly discussed. Some researches on clean sand (e.g. Kuribayashi et al., 1975; Kuwano et al., 1999; Goudarzy et al., 2018b) also reported the decrease of small strain stiffness in constant *p'* shear, and the reason was considered as the abrupt development of shear strain or the start of dilation. Gu et al. (2014) reported that the coordination number at critical state is generally smaller than the initial one, although the density or mean effective stress *p'* at critical state may be higher. This decrease in particle contacts at large strains, especially the radial strain, could possibly lead to the decrease of G_0 at critical state. In any case, lower values of G_0 are expected at critical state with or without fines, and cannot be simply related to the amount of fines. The choice of a unique line for the different fines contents is then reasonable.

Normalised behaviour

Figure 12 shows the data for the small strain stiffness measured during isotropic compression normalised to take account of the effect of the silt on the compressibility and the void ratio. This is achieved by plotting the data in terms of v_n, a normalised specific volume that has been used instead of Burland's (1990) void index to plot data from triaxial tests (e.g. Coop & Cotecchia, 1995; Xu & Coop, 2017). It is defined as:

$$v_{\mathrm{n}} = \exp\left(\frac{\ln(v) - \mathrm{N}^*}{\lambda^*}\right) \quad [3]$$

Where N^* and λ^* were defined in equation [1]. So that by definition:

$$v_{\mathrm{n}} = 1/p' \quad [4]$$

In figure 12a, showing the data points on the $\ln v_n$-$\ln p'$ plane, the NCL is plotted as per equation [4]. The CSL, parallel to the NCL, was derived from the horizontal distance of the CSL to the NCL in the $\ln v$-$\ln p'$ plane, directly calculated from values of N^*, Γ^* and λ^* for each soil mixture. In figure 12b, the small strain stiffness data are plotted in the $\ln v_{\mathrm{n}}$-$\ln G_0$ plane. In order to derive the NCL and CSL in that same plot (fig. 12b), the equations describing the NCL and CSL in the two planes $\ln G_0$-$\ln p'$ and in $\ln v_{\mathrm{n}}$-$\ln p'$ (eq. [2], [3] and the distance between NCL and CSL) are combined to find unique relationships between v_n and G_0 at isotropic compression states and at critical states. They are plotted in figure 12b. The fit is good considering the simplicity of the approach. Any effect of the different pressures and densities of the various samples on the small strain stiffness can further be erased by: (i) normalising G_0 for pressure with respect to the equivalent G_0^* at the same value of p' on the NCL identified in figure 10, and (ii) normalising the value of p' for volume with respect to the equivalent p'_{cs} at the same volume on the CSL identified in figure 12a. This approach was adapted from Jovičić & Coop (1997) to benefit from the better fit of the critical state data points in the volumetric space in this work. It results that all isotropic normally consolidated states are represented by a single point, plotted at at $p'/p'_{cs}{}^* = 2.06$ (the approximate distance between the NCL and CSL) and $G_0/G_0^* = 1.0$, while all critical states are represented by a single point, plotted at $p'/p'_{cs}{}^* = 1.0$ and $G_0/G_0^* = 0.72$, which corresponds to the ratio of intercepts A_{CSL}/A_{NCL}. Figure 13 shows that the data points describing the isotropic compression of the specimens fall on a unique line, reaching a unique isotropic NCL at point ($p'/p'_{cs}{}^* = 2.06$, $G_0/G_0^* = 1.0$) as defined above. The data points describing critical states fall close to a unique CSL at point (($p'/p'_{cs}{}^* = 1.0$, $G_0/G_0^* = 0.72$), also defined above. The small scatter observed was also observed in figure 8, and results from the fact that the NCL and CSL are best-fitted to data that are, inevitably, not perfectly aligned on them. Despite this, the approach validates that defining a unique NCL and CSL for silty sands is possible, once the effects of the fines on the density and compressibility have been taken into account by normalising. Previous attempts to unify data for silty sands took account of the effect of adding silt on the void ratio by using normalising parameters such as the equivalent granular void ratio (e.g. Goudarzy et al., 2016a), or the state parameter (e.g. Yang & Liu, 2016). The advantage of the first approach was to integrate the results within a recognised framework for fines-sand mixtures, but a complex definition of the intergranular void ratio was used, necessitating fitting parameters and therefore rendering the accuracy of the predicted small strain stiffness dependent on the accuracy of the equivalent granular void ratio. The second approach by Yang & Liu (2016) also has the benefit that it uses a well-known parameter, the state parameter, that is included in numerical models for sands, but the combination of tested sands that yield at large stresses with limited ranges of pressures meant that a dependence on the void ratio pre-yield remained. This has been avoided here by ensuring that a unique NCL was reached, so any normalisation was unequivocal.

Conclusions

The presence of fines has traditionally been shown to affect sand behaviour, from the index properties to the small strain stiffness. A crushable sand, pumice, was used as the host sand in this study to reach a unique normal compression line under the conventional pressure levels obtained in laboratory, thus, normalizations under the Critical State Soil Mechanics framework can be applied. This paper has shown that if the behaviours of pure sand and fines-sand mixtures are compared for states where there is a unique relationship between volume and pressure, they can be successfully normalised for composition and volume, cancelling effects the fines may have on the index properties, compressibility and density. The normalised behaviour of the sand-silt mixtures can then be considered as unique.

Acknowledgements

The authors would like to thank Professor Coop at the City University of Hong Kong for enabling the constant p' tests with vertical and horizontal bender element tests to be performed.

Notation

D_{50} mean particle size of the sand

d_{50} mean particle size of the silt

e global void ratio

e_{max} maximum global void ratio

e_{min} minimum global void ratio

e_0 initial global void ratio

e_{final} final global void ratio

FC_t transitional fines content

v specific volume

D_r relative density

σ'_v effective normal stress

p' mean effective stress

p'^* equivalent value of p' taken on the NCL

p'_{cs} mean effective stress at critical state

$p'_{cs}{}^*$ equivalent value of p' taken on the CSL

q deviatoric stress

q_{cs} deviatoric stress at critical state

ε_v volumetric strain

ε_a axial strain

u pore water pressure

u_0 initial pore water pressure

η stress ratio of q/p'

M gradient of CSL in q-p' plane

λ^* gradient of NCL or CSL in ln$v$-lnp' plane

N* intercept of NCL at p'=1kPa in ln$v$-lnp' plane

Γ^* intercept of CSL at p'=1kPa in ln$v$-lnp' plane

G_0 small strain stiffness

$G_0{}^*$ equivalent value of G_0 on the NCL

A soil small strain stiffness parameter

n soil small strain stiffness parameter

v_n normalised specific volume

References

Altuhafi, F. & Coop, M.R. (2011). Changes to particle characteristics associated with the compression of sands. *Géotechnique* **61**, No. 6, 459-471.

Been, K. & Jefferies, M.G. (1985). A state parameter for sands. *Géotechnique* **35**, No. 2, 99-112.

Burland, J.B. (1990). On the compressibility and shear strength of natural clays. Thirtieth Rankine Lecture. *Géotechnique* **40**, No. 3, 329-378.

Butterfield, R. (1979). A natural compression law for soils (an advance on e-logp'). *Géotechnique* **29,** No. 4, 469-480.

Camacho-Tauta, J.F., Cascante, G., Viana da Fonseca, A. & Santos, J.A. (2015). Time and frequency domain evaluation of bender element systems. *Géotechnique* **65**, No. 7, 548-562.

Carrera, A., Coop, M. & Lancellotta, R. (2011). Influence of grading on the mechanical behaviour of Stava tailings. *Géotechnique* **61**, No. 11, 935-946.

Chandler, H.W. (1985). A plasticity theory without Drucker's postulate, suitable for granular materials. *Journal of the Mechanics and Physics of Solids* **33**, No. 3, 215-226.

Coop, M.R. (1990). The mechanics of uncemented carbonate sands. *Géotechnique* **40**, No. 4, 607-626.

Coop, M.R. & Cotecchia, F. (1995). The compression of sediments at the archaeological site of Sibari. *Proc. 11th ECSMFE, Copenhagen, Denmark* 8, 19-26.

Coop, M.R., Sorensen, K.K., Bodas Freitas, T. & Georgoutsos, G. (2004). Particle breakage during shearing of a carbonate sand. *Géotechnique* **54**, No. 3, 157-163.

Dash, H.K., Sitharam, T.G. & Baudet, B.A. (2010). Influence of non-plastic fines on the response of a silty sand to cyclic loading. *Soils and Foundations* **50**, No. 5, 695-704.

Georgiannou, V.N. (2006). The undrained response of sands with additions of particles of various shapes and sizes. *Géotechnique* **56**, No. 9, 639-649.

Goudarzy, M., König, D. & Schanz, T. (2016a). Small strain stiffness of granular materials containing fines. *Soils and Foundations* **56**, No. 5, 756-764.

Goudarzy, M., Rahman, M.M., König, D. & Schanz, T. (2016b). Influence of non-plastic fines content on maximum shear modulus of granular materials. *Soils and Foundations* **56**, No. 6, 973-983.

Goudarzy, M., König, D. & Schanz, T. (2018a). Small and intermediate strain properties of sands containing fines. *Soil Dynamics and Earthquake Engineering* **110**, 110-120.

Goudarzy, M., König, D. & Schanz, T. (2018b). Interpretation of small and intermediate strain characteristics of Hostun sand for various stress states. *Soils and Foundations* **58**, No. 6, 1526-1537.

Gu, X.Q., Huang, M.S., Qian, J.G. (2014). DEM investigation on the evolution of microstructure in granular soils under shearing. *Granular Matter* **16**, No.1, 91-106.

Gudehus, G. (1996). A comprehensive constitutive equation for granular materials. *Soils and Foundations* **36**, No. 1, 1-12.

Ishihara, K. (1996). *Soil behaviour in earthquake geotechnics*, 1st edn. Oxford: Clarendon.

Jovičić, V. & Coop, M.R. (1997). Stiffness of coarse-grained soils at small strains. *Géotechnique* **47**, No. 3, 545-561.

Kenney, T. C. & Lau, D. (1985). Internal stability of granular filters. *Canadian Geotechnical Journal* **22**, No. 2, 215-225.

Klotz, E.U. & Coop, M.R. (2002). On the identification of critical state lines for sands. *ASTM Geotechnical Testing Journal* **25**, No. 3, 289-302.

Kuribayashi, E., Iwasaki, T., Tatsuoka, F. (1975) Effects of stress-strain conditions on dynamic properties of sands. *Proceedings of the Japan Society of Civil Engineers* **1975**, No. 242, 105-114.

Kuwano, R., Connolly, T.M. & Kuwano, J. (1999). Shear stiffness anisotropy measured by multi-directional bender element transducers. *Proc. 2nd Int. Symp. on Pre-failure Deformation Characteristics of Geomaterials, Torino* 1, 205-212.

Lade, P.V., Liggio, Jr. C.D. & Yamamuro, J.A. (1998). Effects of nonplastic fines on minimum and maximum void ratios of sand. *ASTM Geotechnical Testing Journal* **21**, No. 4, 336-347.

Lade, P.V. & Yamamuro, J.A. (1997) Effects of non-plastic fines on static liquefaction of sands. *Canadian Geotechnical Journal* **34**, No.6, 918–928.

Lee, I.K. & Coop, M.R. (1995). The intrinsic behaviour of a decomposed granite soil. *Géotechnique* **45**, No. 1, 117-130.

Liu, X., Yang, J., Wang, G.H., Chen, L.Z. (2016). Small-strain shear modulus of volcanic granular soil: An experimental investigation. *Soil Dynamics and Earthquake Engineering* **86**, 15-24.

Liu, X. & Yang, J. (2018). Shear wave velocity in sand: effect of grain shape. *Géotechnique* **68**, No. 8, 742-748, **doi**: 10.1680/jgeot.17.T.011.

McDowell, G.R. & Bolton, M.D. (1998). On the micromechanics of crushable aggregates. *Géotechnique* **48**, No. 5, 667-679.

Muszynski, M.R. (2006). Determination of maximum and minimum densities of poorly graded sands using a simplified method. *ASTM Geotechnical Testing Journal* **29**, No. 3, 1–10.

Minh, N.H., Cheng, Y.P. & Thornton, C. (2014). Strong force networks in granular mixtures. *Granular Matter* **16**, No. 1, 69-78.

O’Donovan, J., O’Sullivan, C., Marketos, G. & Muir Wood, D. (2015). Analysis of bender element test interpretation using the discrete element method. *Granular Matter* **17,** No. 2, 197-216.

Payan, M., Senetakis, K., Khoshghalb, A., Khalili, N. (2017). Characterization of the small-strain dynamic behaviour of silty sands; contribution of silica non-plastic fines content. *Soil Dynamics and Earthquake Engineering* **102**, 232-240.

Polito, C.P. & Martin, J.R. (2001). Effects of nonplastic fines on the liquefaction resistance of sands. *ASCE Journal of Geotechnical and Geoenvironmental Engineering* **127**, No. 5, 408-415.

Ponzoni, E., Nocilla, A. & Coop, M.R. (2017). The behaviour of a gap graded sand with mixed mineralogy. *Soils and Foundations* **57**, No. 6, 1030-1044.

Prashant, A., Bhattacharya., D. & Gundlapalli, S. (2019). Stress-state dependency of small-strain shear modulus in silty sand and sandy silt of Ganga. *Géotechnique* **69**, No. 1, 42-56, **doi**: 10.1680/jgeot.17.P.100.

Rocchi, I. & Coop, M. R. (2014). Experimental accuracy of the initial specific volume. Geotech. Testing J. **37**, No. 1, 169–175.

Salgado, R., Bandini, P. & Karim, A. (2000). Shear strength and stiffness of silty sand. *ASCE Journal of Geotechnical and Geoenvironmental Engineering* **126**, No. 5, 451-462.

Shipton, B. & Coop, M.R. (2012). On the compression behaviour of reconstituted soils. *Soils and Foundations* **52**, No. 4, 668-681.

Shipton, B. & Coop, M.R. (2015). Transitional Behaviour in Sands with Plastic and Non-plastic Fines. *Soils and Foundations* **55**, No. 1, 1-16.

Shire, T., O’Sullivan, C., Hanley, K.J. & Fannin, R.J. (2014). Fabric and Effective Stress Distribution in Internally Unstable Soils. *ASCE Journal of Geotechnical and Geoenvironmental Engineering* **140**, No. 12, 04014072

Shire, T., O'Sullivan, C., Hanley, K.J. (2016). The influence of fines content and size-ratio on the micro-scale properties of dense bimodal materials. *Granular Matter* **18**, No.3, 1-10.

Thevanayagam, S., Shenthan, T., Mohan, S. & Liang, J. (2002). Undrained fragility of clean sands, silty sands, and sandy silts. *ASCE Journal of Geotechninal and Geoenviromental Engineering* **128**, No. 10, 849-859.

To, H.D., Torres, S.A.G., Scheuermann, A. (2014). Primary fabric fraction analysis of granular soils. *Acta Geotechnica* **10**, No. 3, 375–387.

Viggiani, G. & Atkinson, J.H. (1995). Stiffness of fine-grained soil at very small strains. *Géotechnique* **45**, No. 2, 249-265.

Vilhar, G., Jovicic, V. & Coop, M.R. (2013). The role of particle breakage in the mechanics of a non-plastic silty sand. *Soils and Foundations* **53**, No. 1, 91–104.

Voivret, C., Radjai, F., Delenne, J-Y. & El Youssoufi, M.S. (2009). Multiscale Force Networks in Highly Polydisperse Granular Media. *Physical Review Letters* **102**, No. 17, 178001**.**

Wichtmann, T., Navarrete Hernández, M.A. & Triantafyllidis, T. (2015). On the influence of a non-cohesive fines content on small strain stiffness, modulus degradation and damping of quartz sand. *Soil Dynamics and Earthquake Engineering* **69**, 103-114.

Xu, L. & Coop, M. R. (2017). The mechanics of a saturated silty loess with a transitional mode. *Géotechnique* **67**, No. 7, 581-596.

Yang S., Lacasse, S. & Sandven, R. (2006). Determination of the transitional fines content of mixtures of sand and non-plastic fines. *ASTM Geotechnical Testing Journal* **29**, No. 2, 102–107.

Yang, J. & Liu, X. (2016). Shear wave velocity and stiffness of sand: the role of non-plastic fines. *Géotechnique* **66**, No. 6, 500-514.

Zuo, L. & Baudet, B.A. (2015). Determination of the transitional fines content. *Soils and Foundations* **55**, No. 1, 213-219.

Table 1 Summary of tests conducted with silt-pumice mixtures

host sand	test type	sample diameter (mm)	bender element test	fines content (%)	e_0	e_{final}	maximum $\sigma'_v/p'/p'_{cs}$ (kPa)
pumice	OED	50	No	0	1.529, 1.457	0.609, 0.576	6500
				30	1.121, 1.018	0.585, 0.563	
				50	0.744, 0.712	0.498, 0.443	
				60	0.709, 0.554	0.525, 0.386	
	ISO	50	Yes	0	1.584, 1.537, 1.512, 1.477	1.134, 1.128, 1.126, 1.125	1600
				30	1.248, 1.151	0.812, 0.777	
				50	0.836, 0.802	0.647, 0.618	
				60	0.876, 0.767	0.652, 0.632	
	CID	38	No	0	1.538, 1.430	1.269, 1.024	413.8, 604.4
				30	1.144,1.065	0.866, 0.786	411.9, 618.4
				50	0.772, 0.763	0.667, 0.663	420.8, 599.9
				60	0.748, 0.742	0.668, 0.692	412.7, 606.2
		50	Yes	0	1.394	0.974	843.4
				30	0.993	0.692	907.1
				50	0.709	0.631	905.6
				60	0.679	0.632	846.2
pumice	CIU	38	No	0	1.203	same as e_0	192.6
				30	0.952		145.5
				50	0.707		85.9
				60	0.715		108.7
		50	Yes	0	1.477		194.7
				30	1.093		122.6
				50	0.739		53.1
				60	0.701		39.5
	constant p'	50	Yes	0	1.478	1.380	400
				30	1.020	0.902	
				50	0.711	0.667	
				60	0.661	0.644	

OED: oedometer test; ISO: isotropic compression test; CID: drained shearing test; CIU: undrained shearing test

List of figures

Figure 13 Small strain stiffness data during isotropic compression and shearing, normalised with respect to volume


S3400-8658 20.0kV 11.0mm x40 BSECOMP 90Pa
1.00mm
(a)
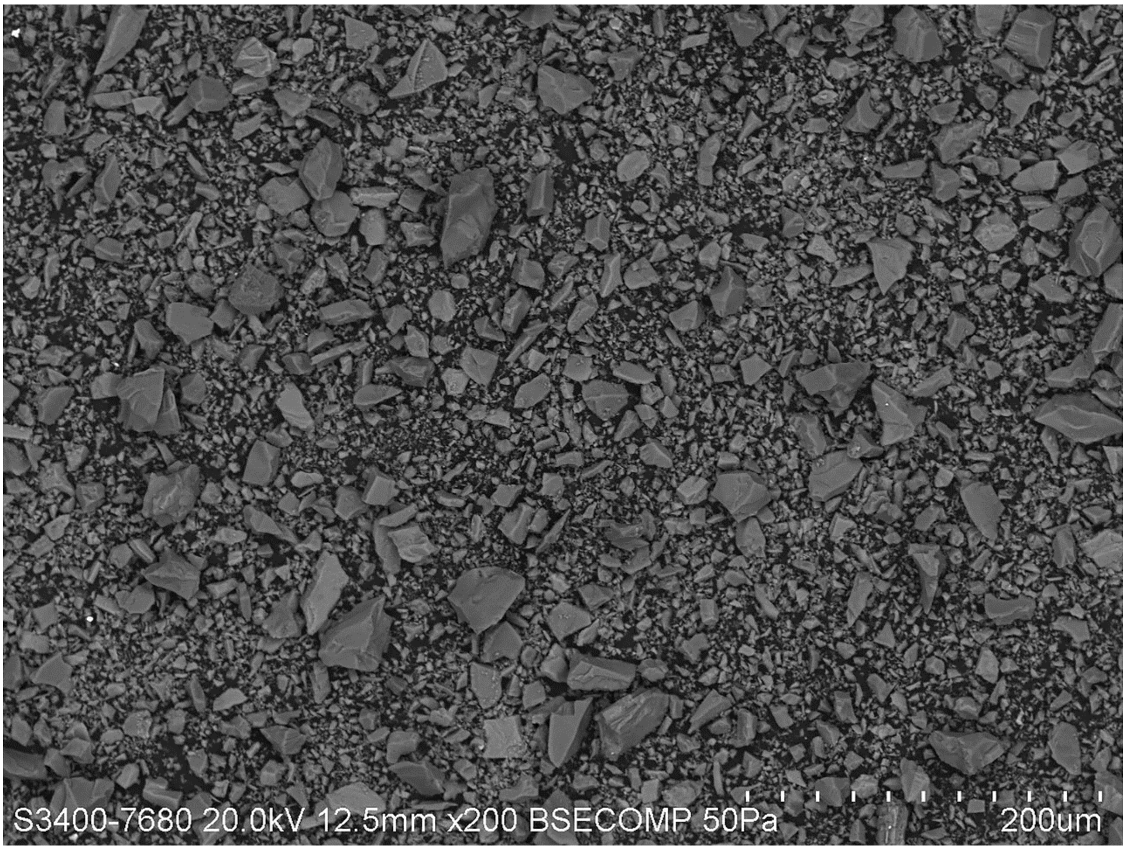
S3400-7680 20.0kV 12.5mm x200 BSECOMP 50Pa
200um
(b)
Figure 1

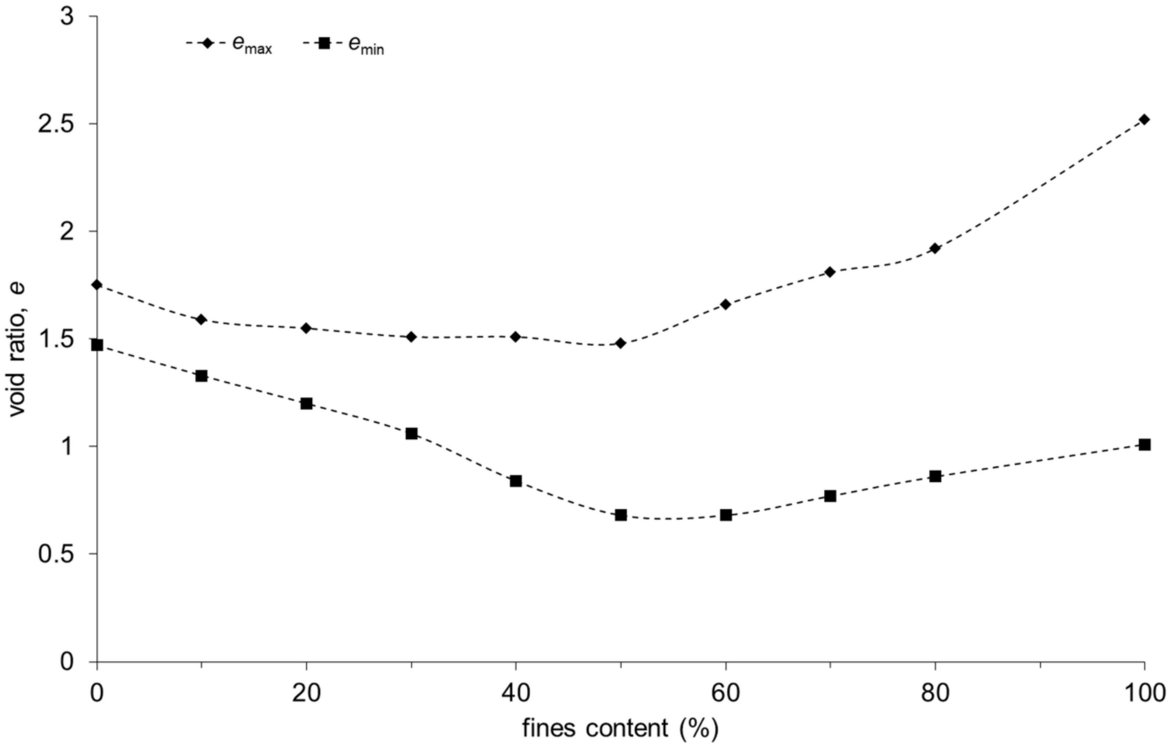
3
2.5
2
1.5
1
0.5
0
void ratio, e
e_{max}
e_{min}
0
20
40
60
80
100
fines content (%)

Figure 2

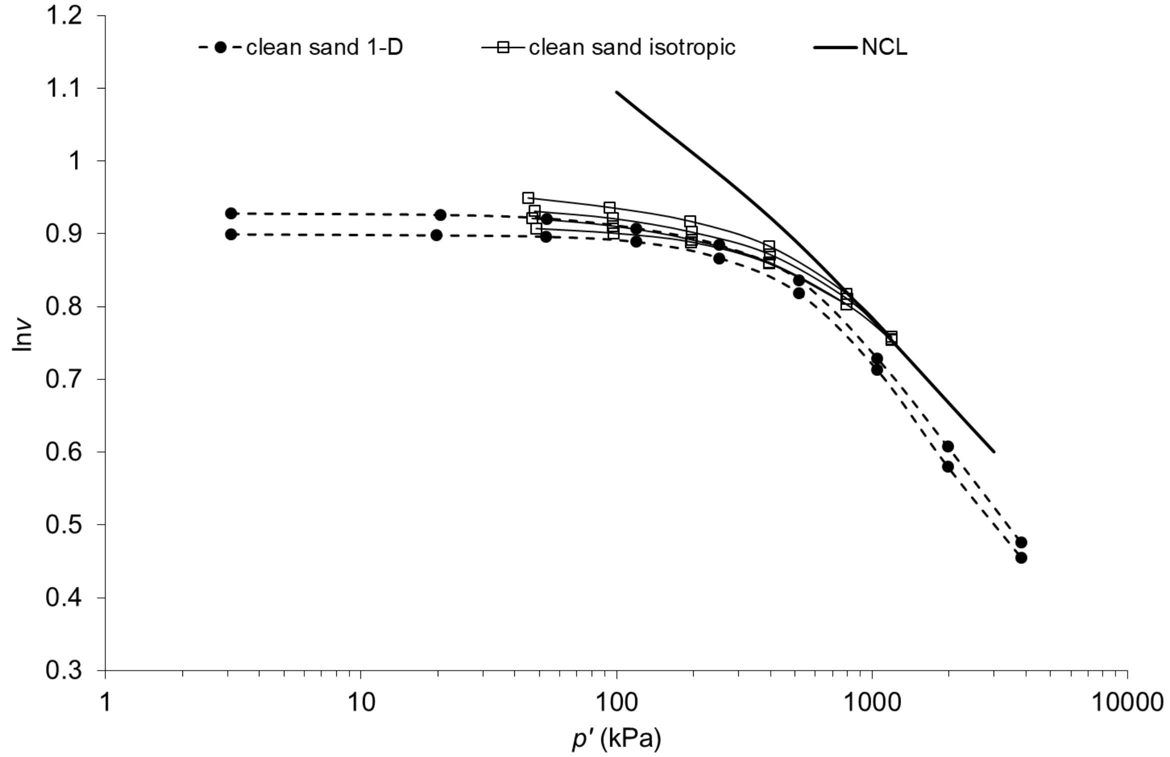
clean sand 1-D
clean sand isotropic
NCL
1.2
1.1
1
0.9
0.8
0.7
0.6
0.5
0.4
0.3
lnv
1
10
100
1000
10000
p' (kPa)

(a)

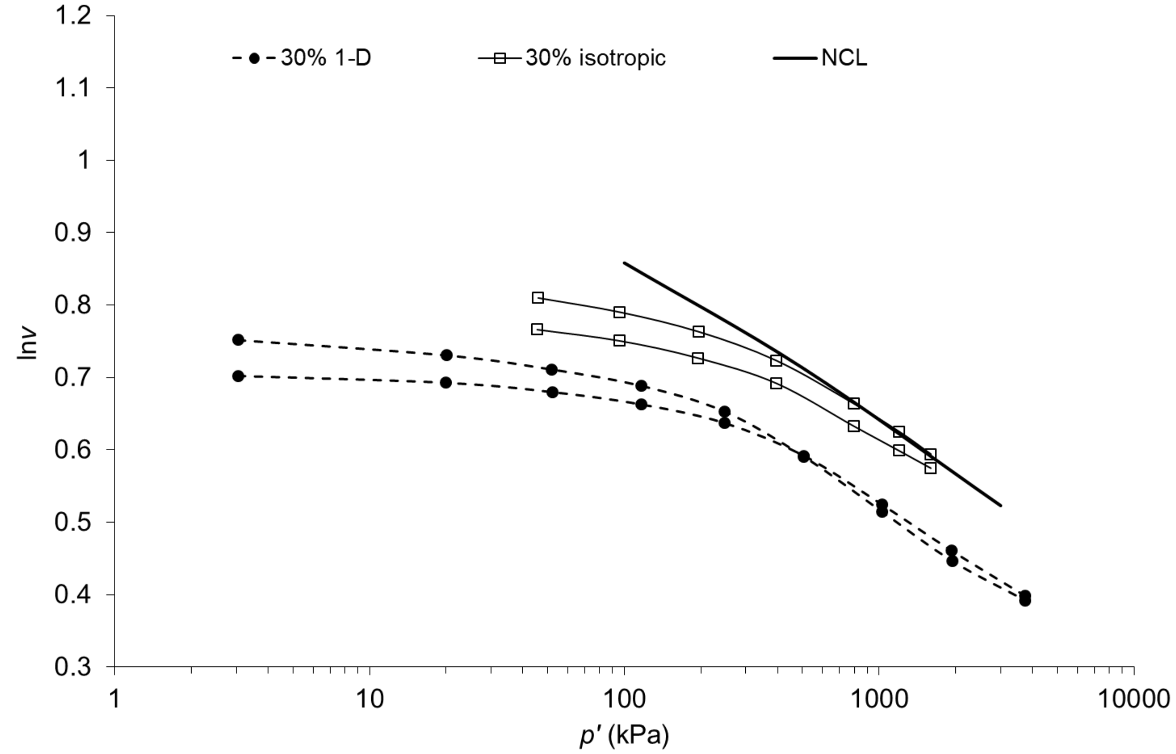
30% 1-D
30% isotropic
NCL
1.2
1.1
1
0.9
0.8
0.7
0.6
0.5
0.4
0.3
lnv
1
10
100
1000
10000
p' (kPa)

(b)

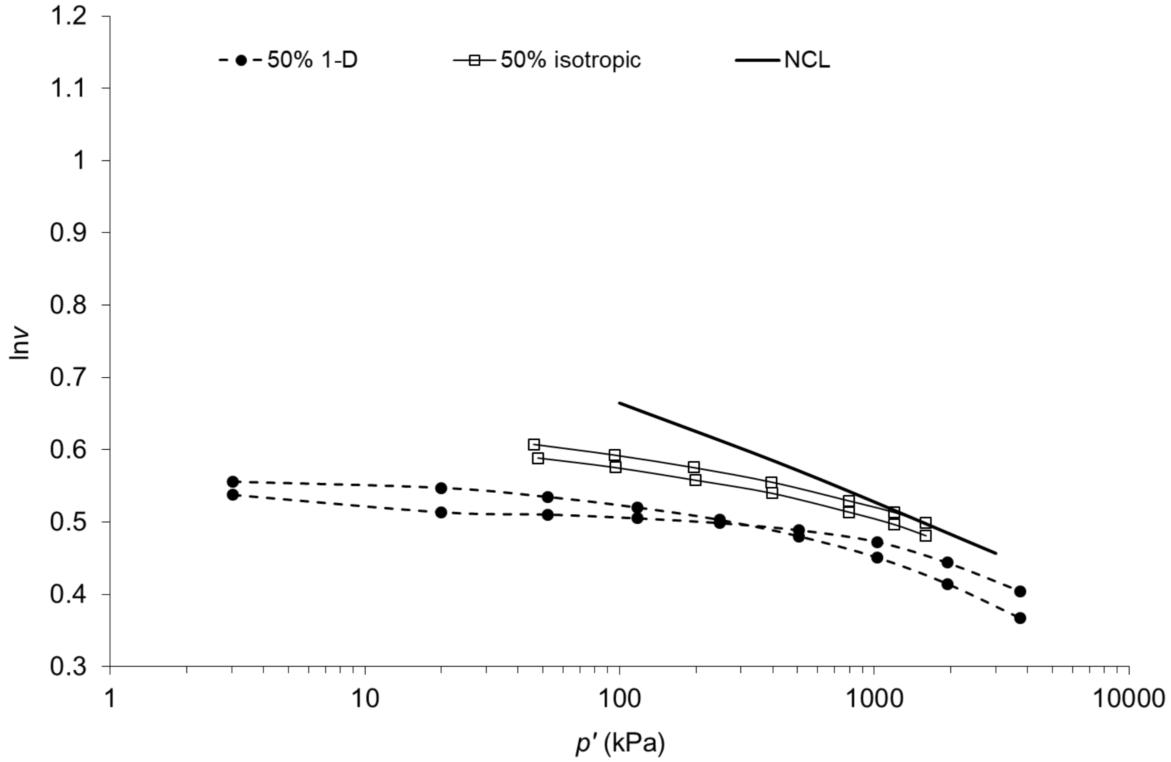
50% 1-D
50% isotropic
NCL
lnv
p′ (kPa)
1.2
1.1
1
0.9
0.8
0.7
0.6
0.5
0.4
0.3
1
10
100
1000
10000

(c)

Figure 3

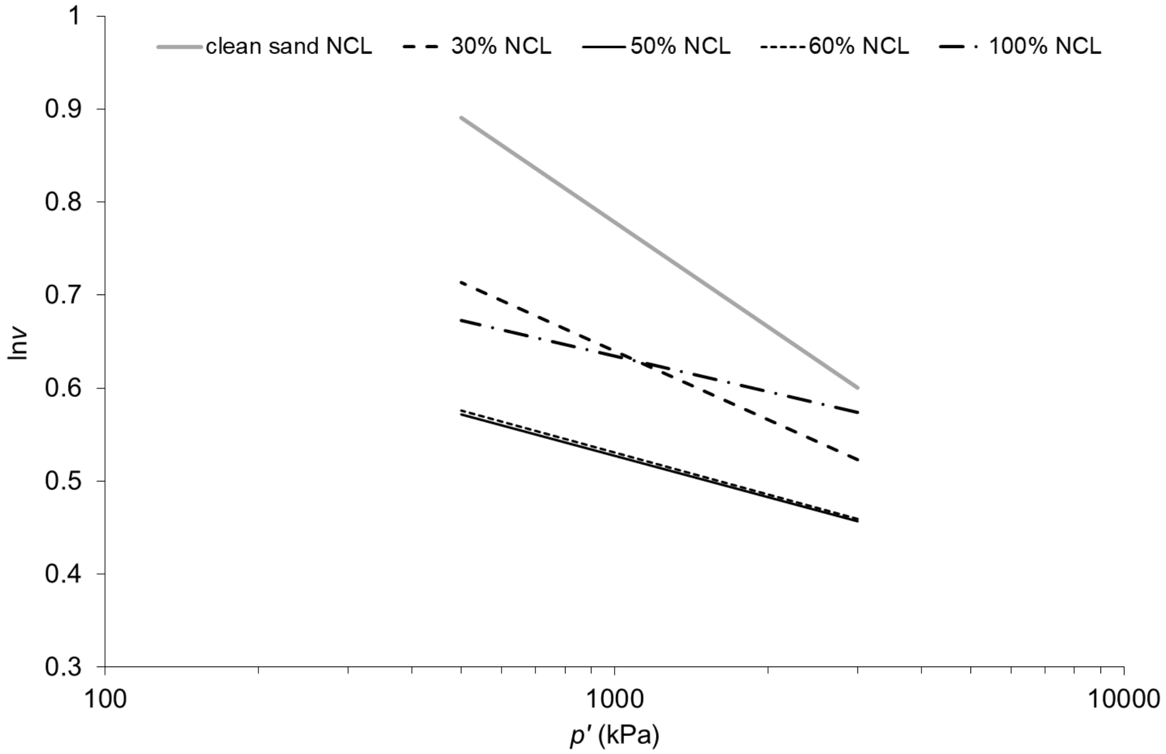
clean sand NCL
30% NCL
50% NCL
60% NCL
100% NCL
1
0.9
0.8
0.7
0.6
0.5
0.4
0.3
lnv
100
1000
10000
p′ (kPa)

Figure 4

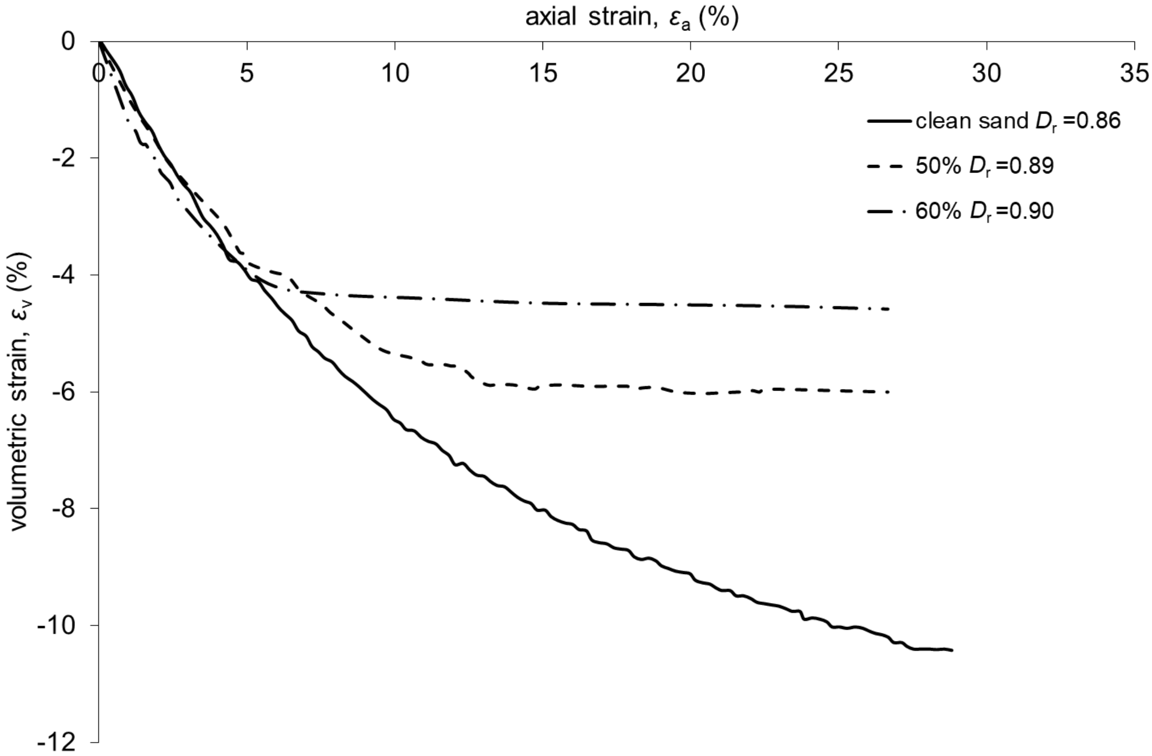
axial strain, ε_a (%)
0
5
10
15
20
25
30
35
-2
-4
-6
-8
-10
-12
volumetric strain, ε_v (%)
clean sand D_r =0.86
50% D_r =0.89
60% D_r =0.90

(a)

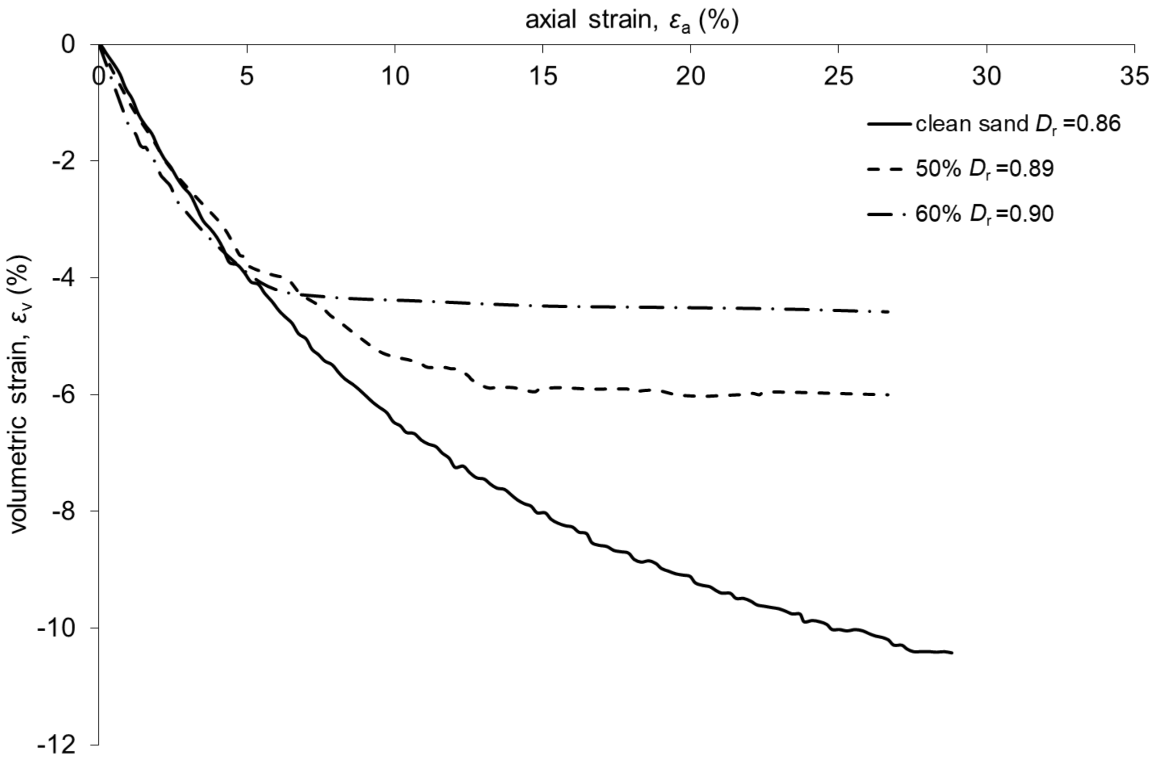
axial strain, ε_a (%)
0
5
10
15
20
25
30
35
-2
-4
-6
-8
-10
-12
volumetric strain, ε_v (%)
clean sand D_r =0.86
50% D_r =0.89
60% D_r =0.90

(b)

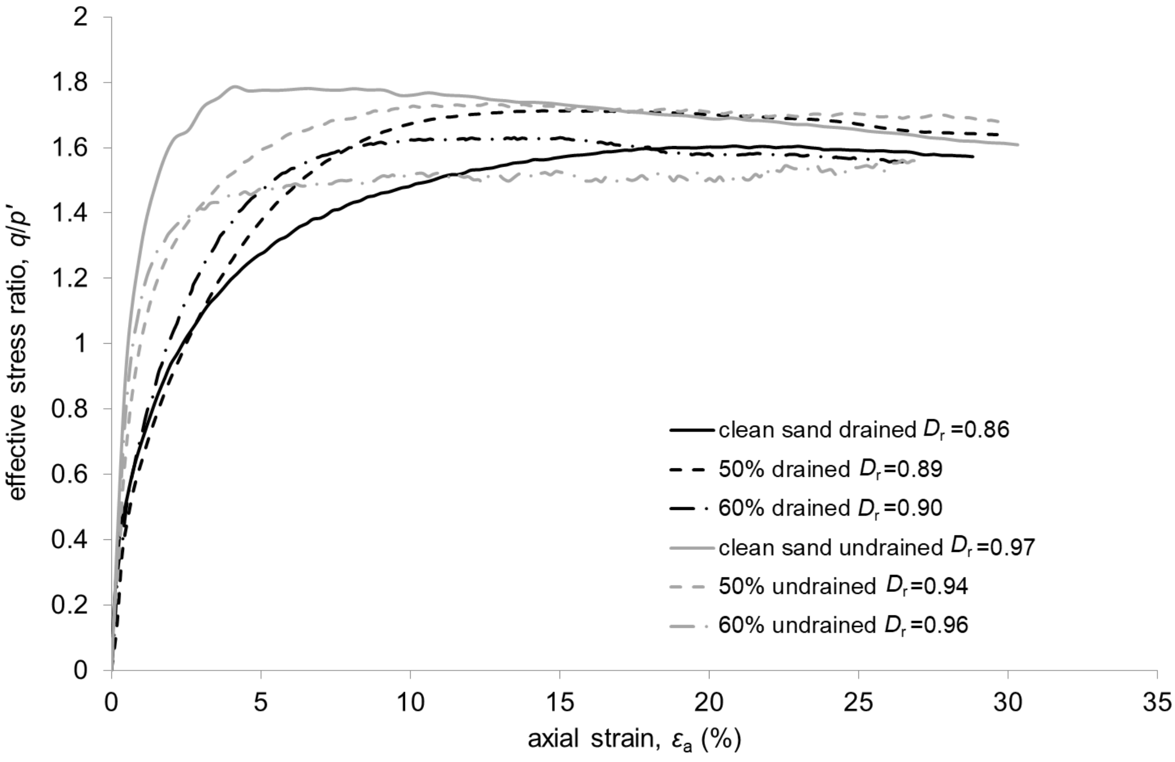

effective stress ratio, q/p'
axial strain, εa (%)
0
0.2
0.4
0.6
0.8
1
1.2
1.4
1.6
1.8
2
0
5
10
15
20
25
30
35
clean sand drained Dr =0.86
50% drained Dr=0.89
60% drained Dr=0.90
clean sand undrained Dr=0.97
50% undrained Dr=0.94
60% undrained Dr=0.96

(c)

Figure 5

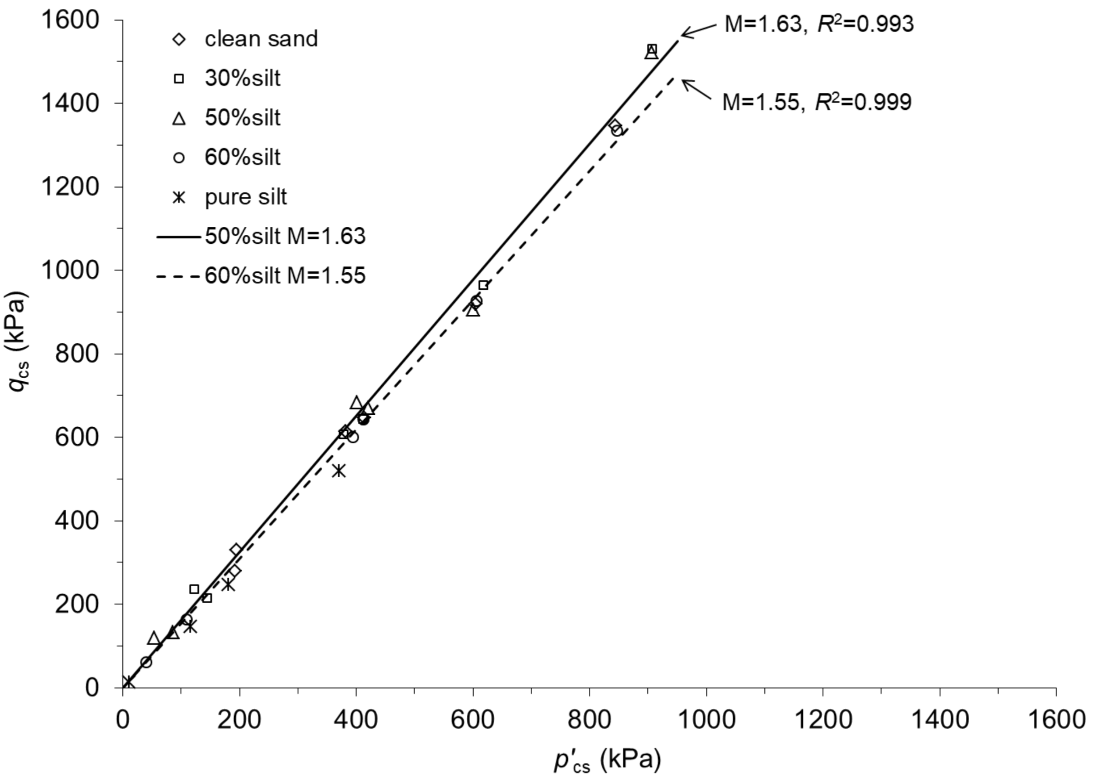
M=1.63, R^2=0.993
M=1.55, R^2=0.999
clean sand
30%silt
50%silt
60%silt
pure silt
50%silt M=1.63
60%silt M=1.55
q_{cs} (kPa)
p'_{cs} (kPa)

(a)

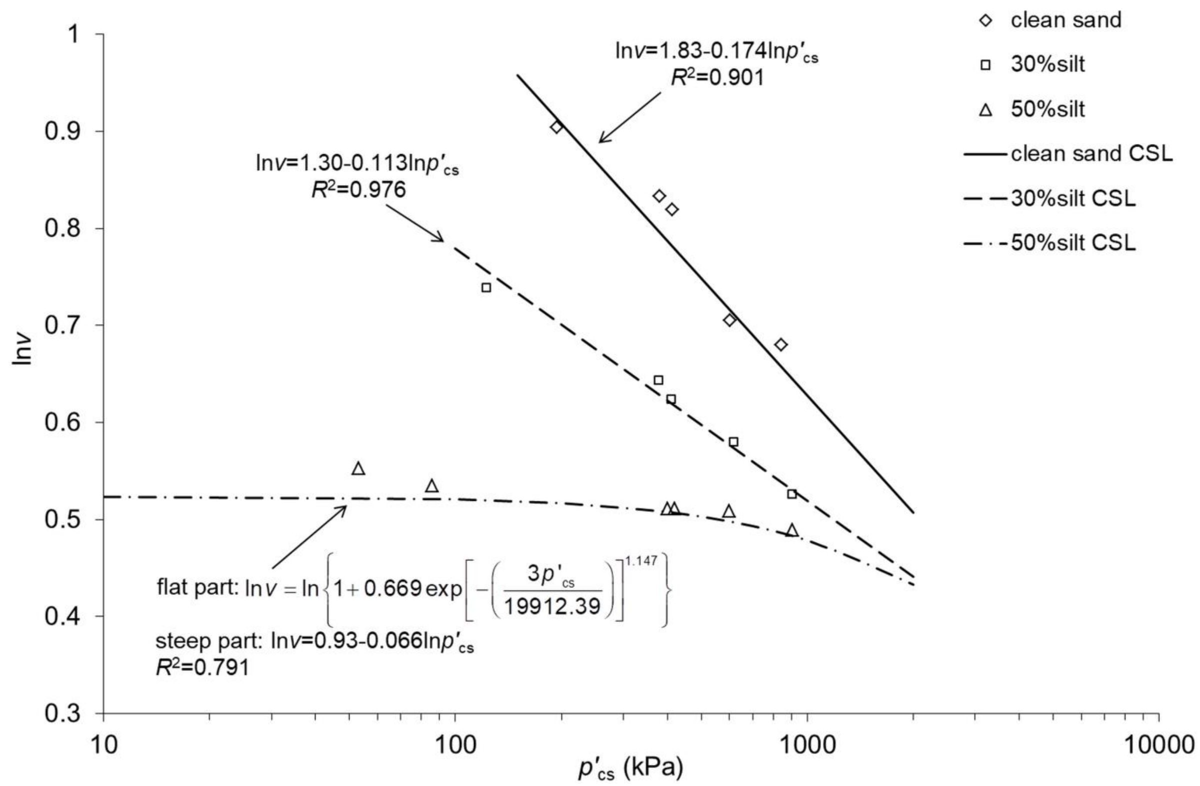
clean sand
30%silt
50%silt
clean sand CSL
30%silt CSL
50%silt CSL
ln$v$=1.83-0.174lnp'_{cs}
R^2=0.901
ln$v$=1.30-0.113lnp'_{cs}
R^2=0.976
flat part: $\ln v = \ln\left\{1 + 0.669\exp\left[-\left(\frac{3p'_{cs}}{19912.39}\right)\right]^{1.147}\right\}$
steep part: ln$v$=0.93-0.066lnp'_{cs}
R^2=0.791
ln$v$
p'_{cs} (kPa)

(b-i)

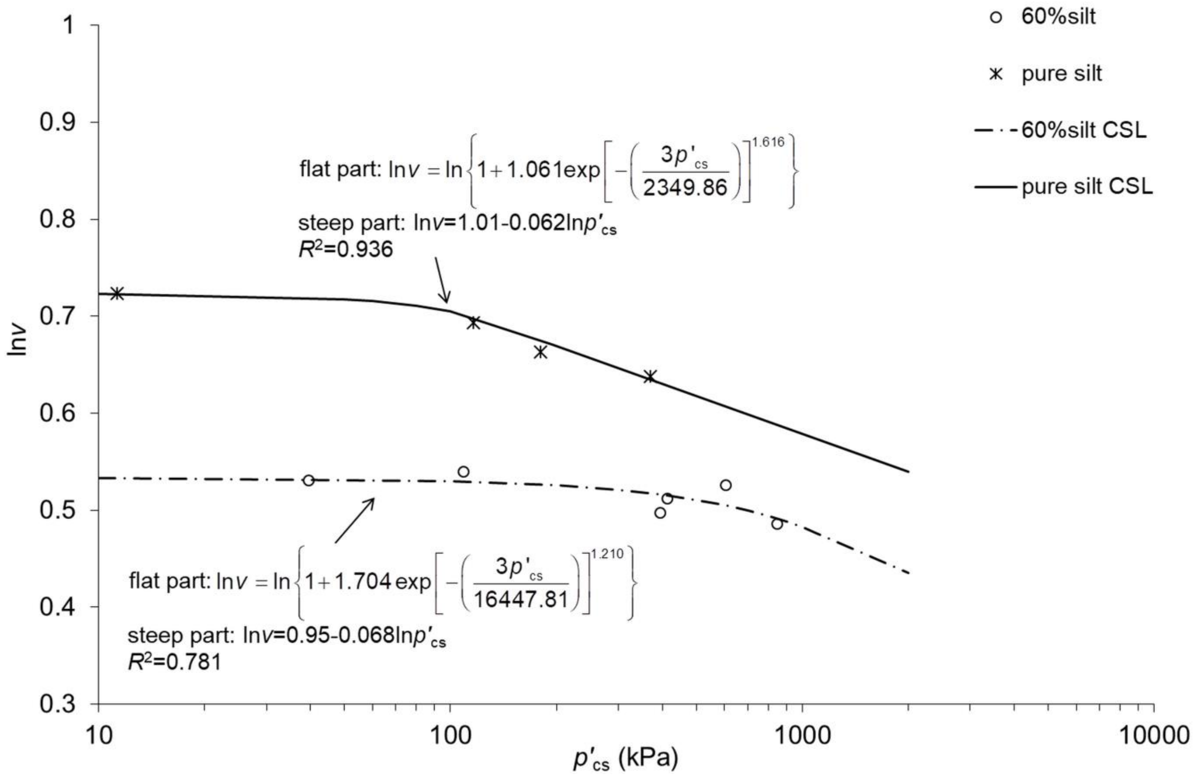

60%silt
pure silt
60%silt CSL
pure silt CSL
flat part: $\ln v = \ln\left\{1+1.061\exp\left[-\left(\frac{3p'_{cs}}{2349.86}\right)\right]^{1.616}\right\}$
steep part: $\ln v$=1.01-0.062$\ln p'_{cs}$
R^2=0.936
flat part: $\ln v = \ln\left\{1+1.704\exp\left[-\left(\frac{3p'_{cs}}{16447.81}\right)\right]^{1.210}\right\}$
steep part: $\ln v$=0.95-0.068$\ln p'_{cs}$
R^2=0.781
$\ln v$
p'_{cs} (kPa)

(b-ii)

Figure 6

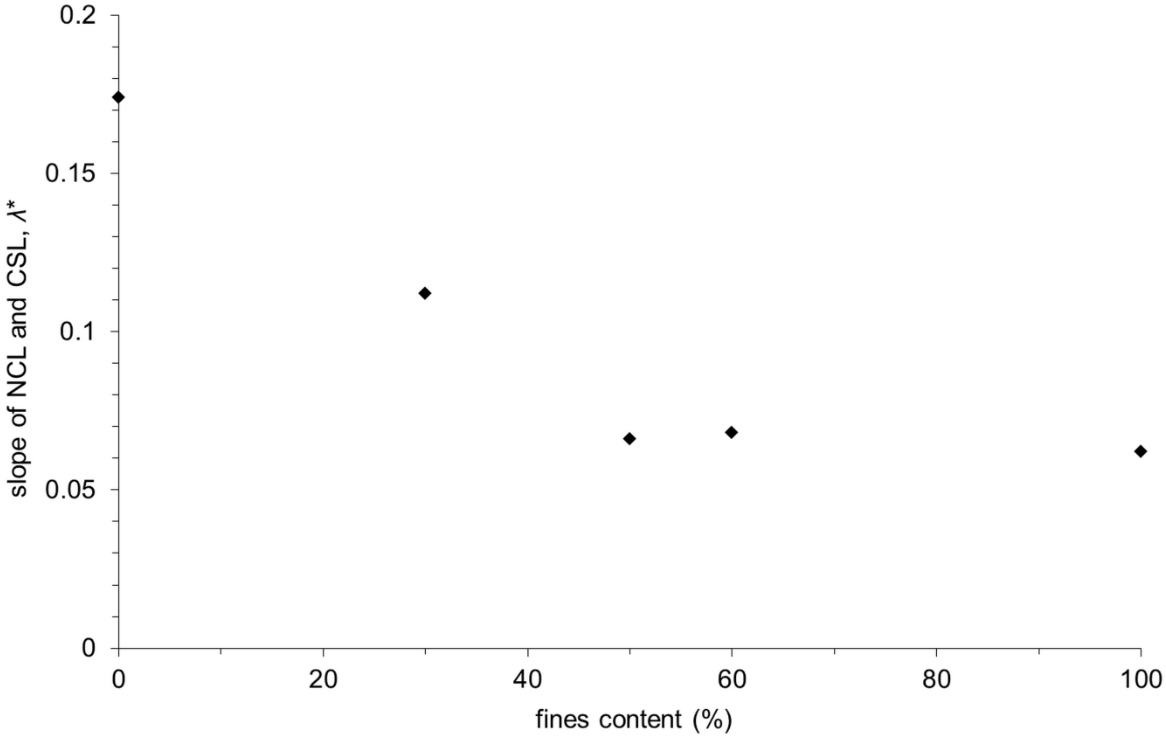

0.2
0.15
0.1
0.05
0
slope of NCL and CSL, λ*
0
20
40
60
80
100
fines content (%)

(a)

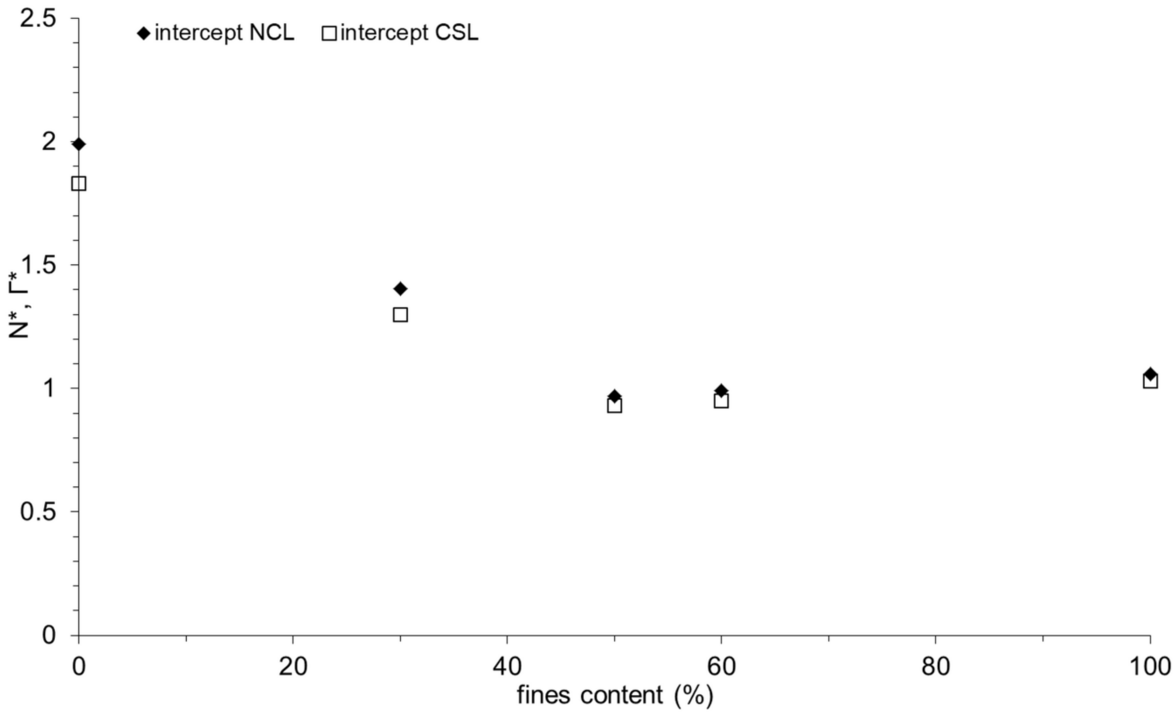

intercept NCL
intercept CSL
2.5
2
1.5
1
0.5
0
N*, Γ*
0
20
40
60
80
100
fines content (%)

(b)

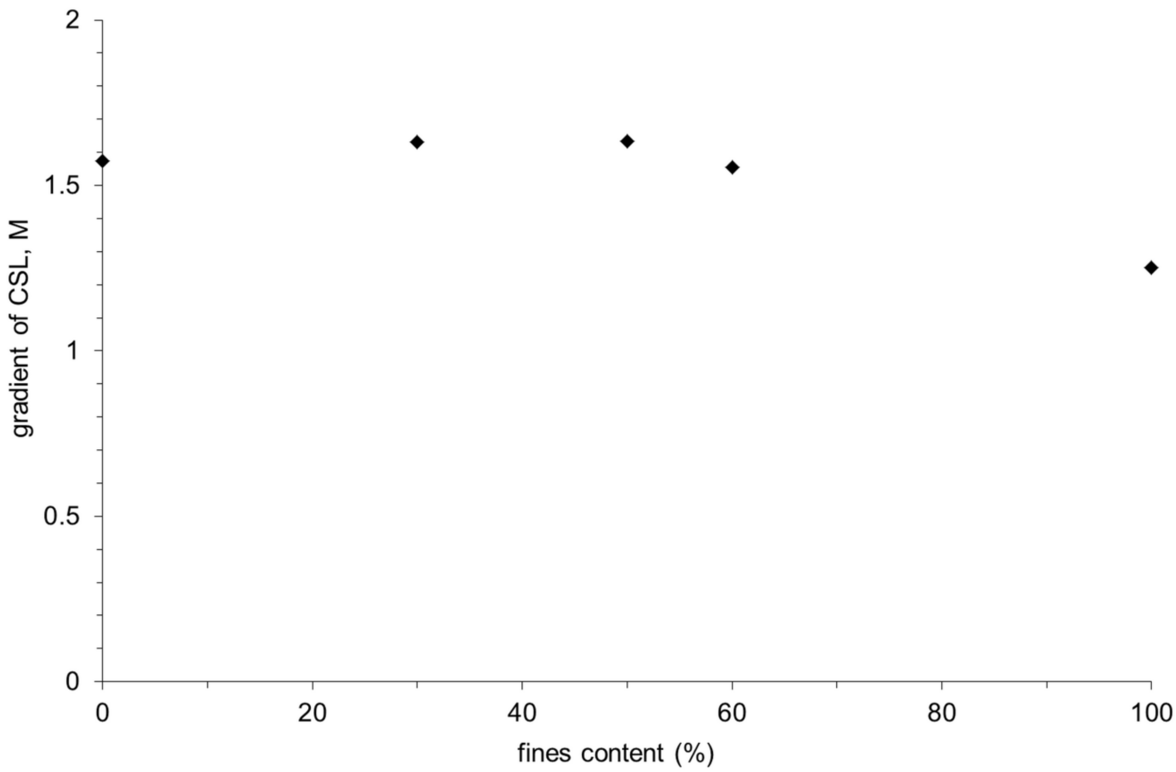

(c)

Figure 7

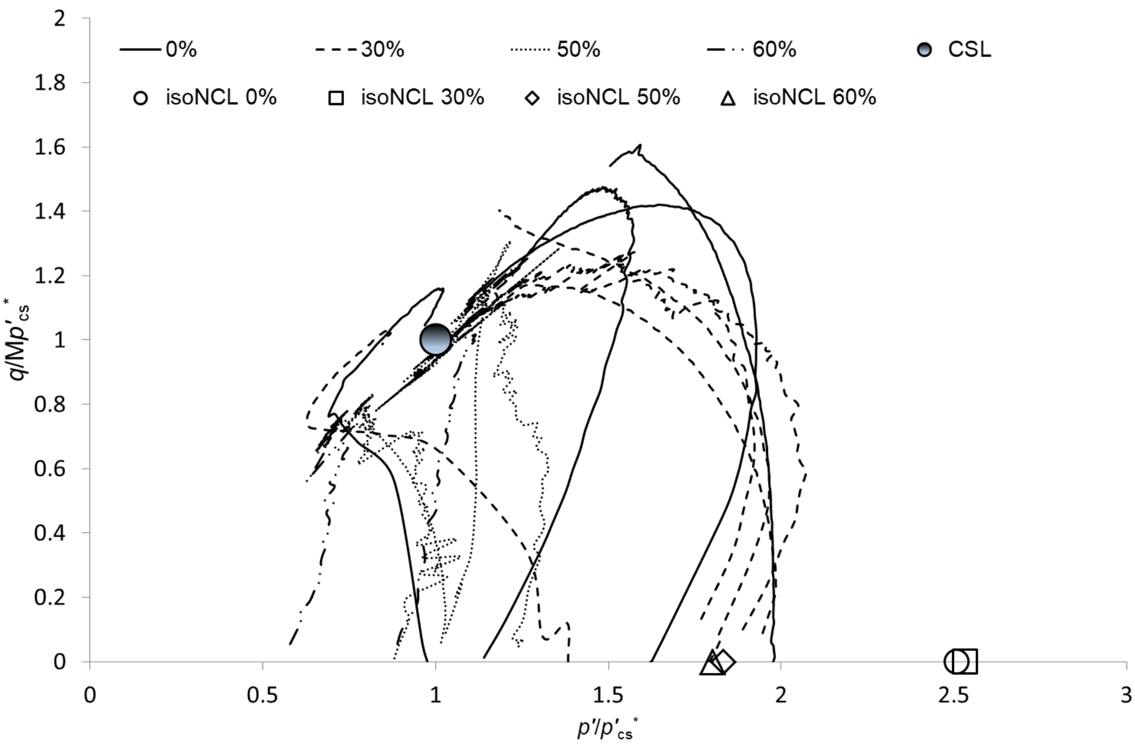

0%
30%
50%
60%
CSL
isoNCL 0%
isoNCL 30%
isoNCL 50%
isoNCL 60%
$q/Mp'_{cs}{}^{*}$
$p'/p'_{cs}{}^{*}$
0
0.2
0.4
0.6
0.8
1
1.2
1.4
1.6
1.8
2
0.5
1.5
2.5
3

Figure 8

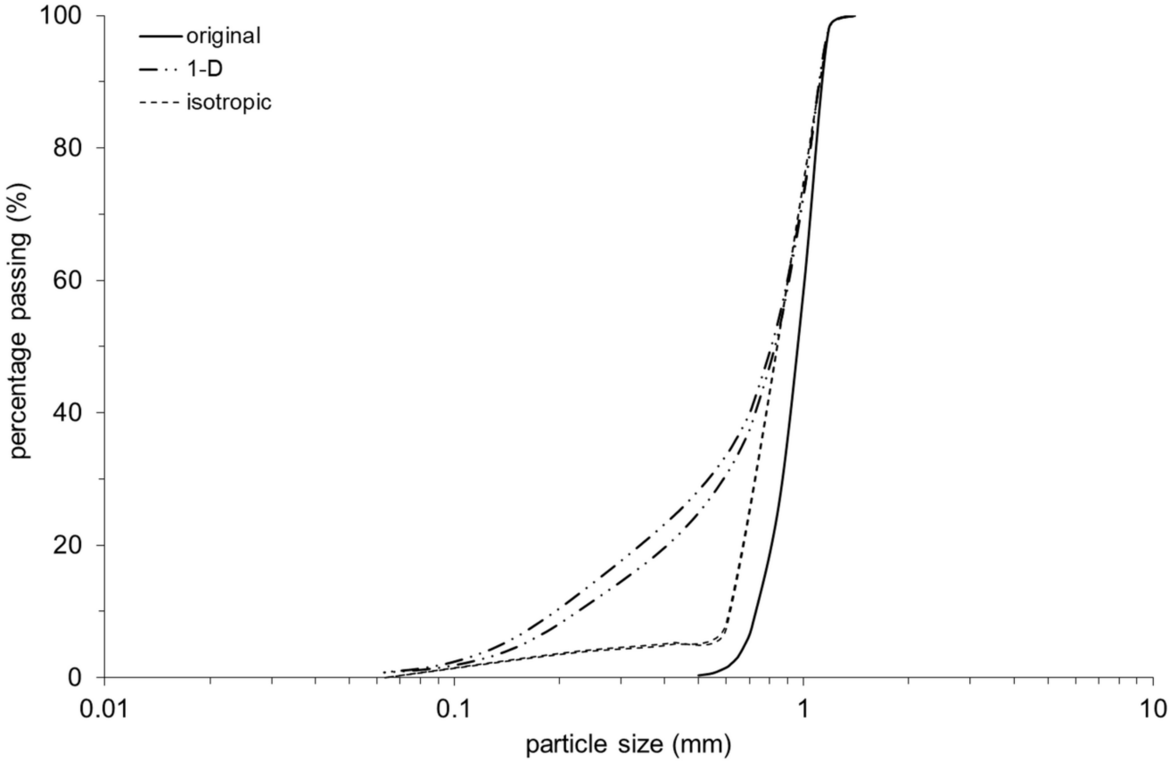
original
1-D
isotropic
100
80
60
40
20
0
percentage passing (%)
0.01
0.1
1
10
particle size (mm)

(a)

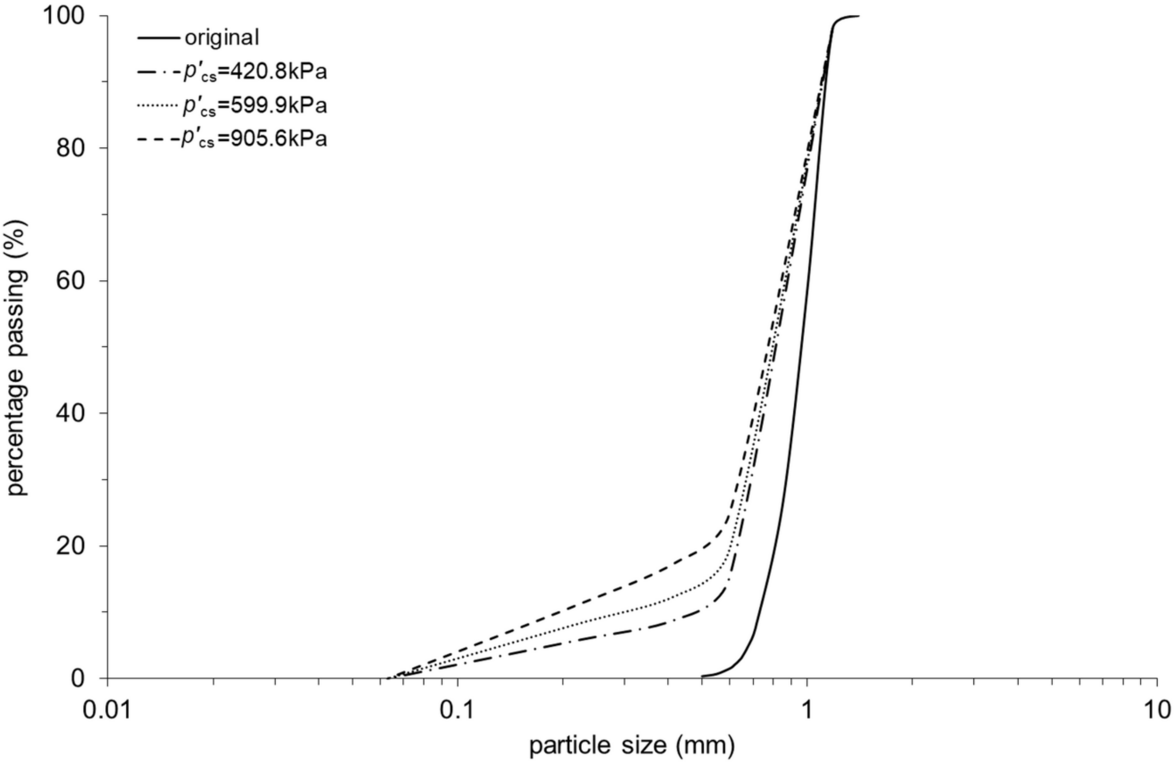
original
p'_{cs}=420.8kPa
p'_{cs}=599.9kPa
p'_{cs}=905.6kPa
100
80
60
40
20
0
percentage passing (%)
0.01
0.1
1
10
particle size (mm)

(b)

Figure 9

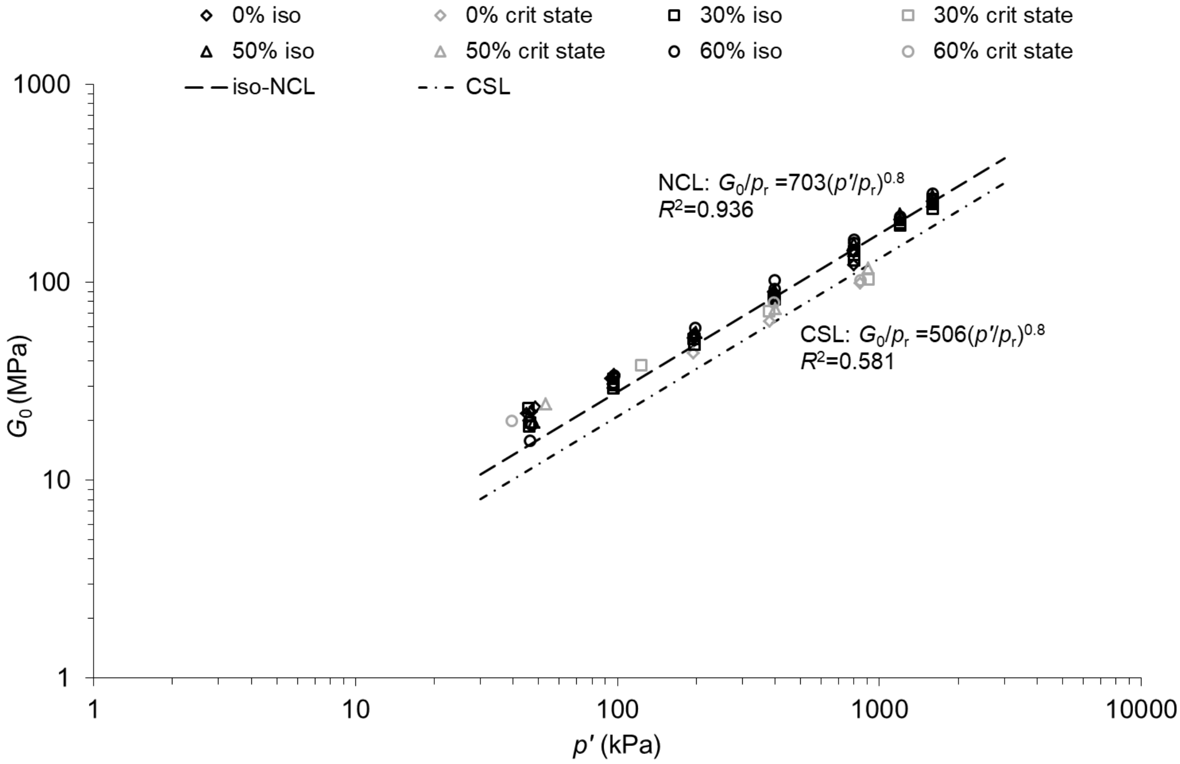
0% iso
0% crit state
30% iso
30% crit state
50% iso
50% crit state
60% iso
60% crit state
iso-NCL
CSL
NCL: $G_0/p_r = 703(p'/p_r)^{0.8}$
R^2=0.936
CSL: $G_0/p_r = 506(p'/p_r)^{0.8}$
R^2=0.581
G_0 (MPa)
p' (kPa)
1000
100
10
1
1
10
100
1000
10000

Figure 10

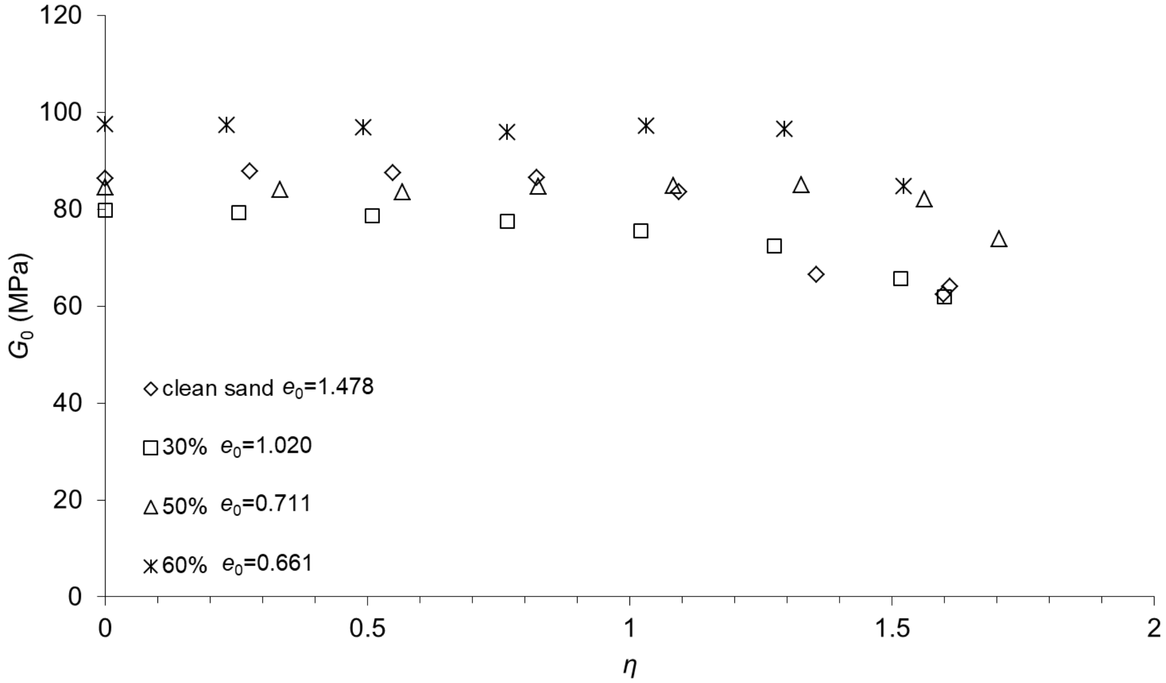

120
100
80
60
40
20
0
G_0 (MPa)
◇ clean sand e_0=1.478
□ 30% e_0=1.020
△ 50% e_0=0.711
✳ 60% e_0=0.661
0
0.5
1
1.5
2
η

Figure 11

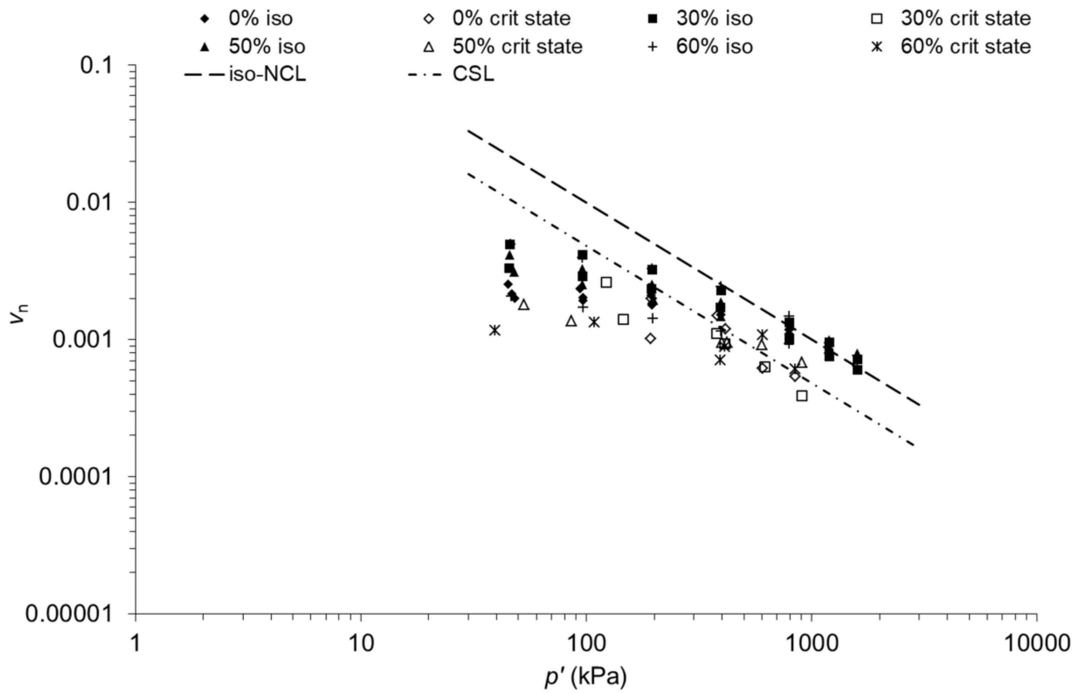
0% iso
0% crit state
30% iso
30% crit state
50% iso
50% crit state
60% iso
60% crit state
iso-NCL
CSL
0.1
0.01
0.001
0.0001
0.00001
v_n
1
10
100
1000
10000
p' (kPa)

(a)

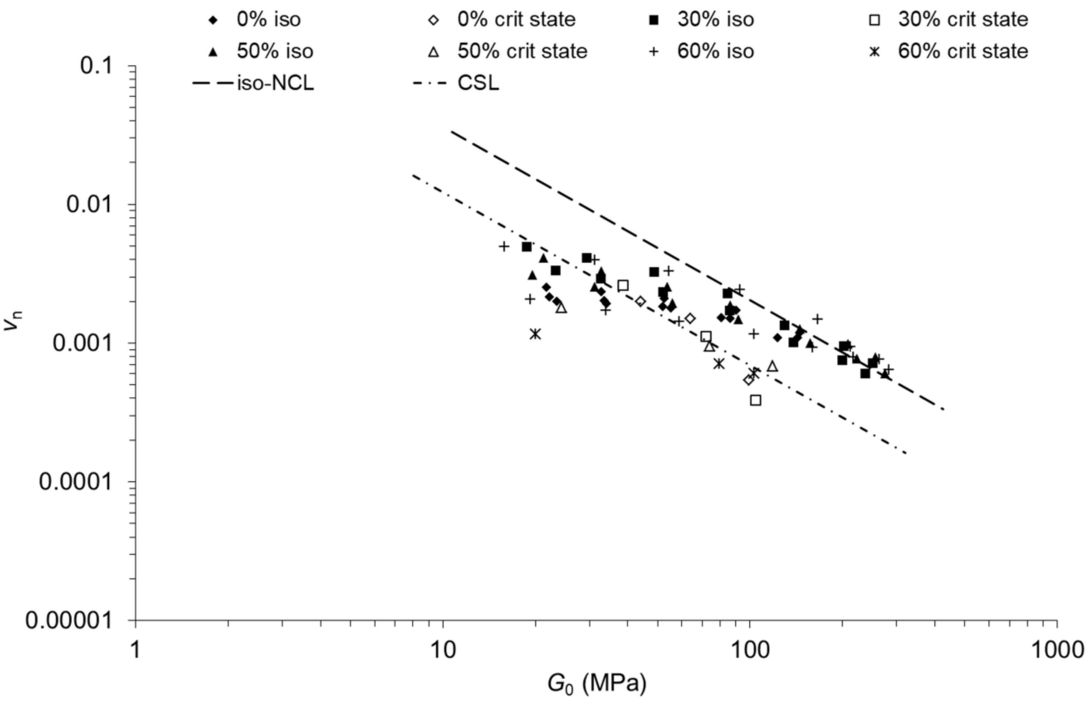
0% iso
0% crit state
30% iso
30% crit state
50% iso
50% crit state
60% iso
60% crit state
iso-NCL
CSL
0.1
0.01
0.001
0.0001
0.00001
v_n
1
10
100
1000
G_0 (MPa)

(b)

Figure 12

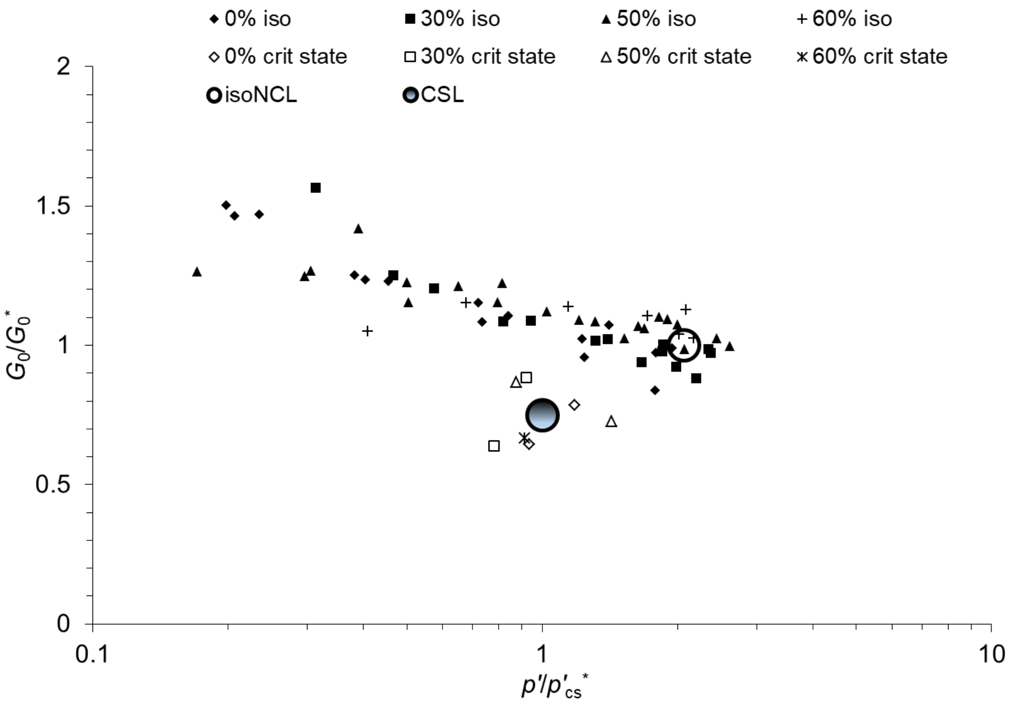
0% iso
30% iso
50% iso
60% iso
0% crit state
30% crit state
50% crit state
60% crit state
isoNCL
CSL
2
1.5
1
0.5
0
0.1
1
10
G_0/G_0^*
$p'/p'_{cs}{}^*$

Figure 13